Borisova et al. (2026)
Melt viscosity as a principal factor controlling the dissolution rates of the lithosphere minerals in planetary and geological melts. A review and perspectives
Advances in Geochemistry and Cosmochemistry 2(1): 964, https://doi.org/10.33063/agc.v2i1.964

Review article

Melt viscosity as a principal factor controlling the dissolution rates of the lithosphere minerals in planetary and geological melts. A review and perspectives

Anastassia Borisova[1]✉ Jacques Schott[1] Michael J. Toplis[2]

[1] Géosciences Environnement Toulouse, GET, Université de Toulouse, UPS, CNRS, IRD, CNES, Toulouse, France
[2] Institut de Recherche en Astrophysique et Planétologie (IRAP), Université de Toulouse, UPS, CNRS, Toulouse, France

✉ **Correspondence to:** Anastassia Borisova: anastassia.borisova-pokrovski@cnrs.fr

Author contributions: Conceptualization: AB, JS, MJT; Data curation: AB; Formal analysis: AB; Funding acquisition: AB; Investigation: AB, JS, MJT; Methodology: AB, JS; Project administration: AB; Resources: AB; Software: AB; Supervision: AB; Validation: AB, JS, MJT; Visualization: AB, JS; Writing – original draft: AB, JS, MJT; Writing – review & editing: AB, JS, MJT.

Data, code, and outputs: https://doi.org/10.5281/zenodo.18607217

Submitted: 2025-08-12
Accepted: 2026-02-07
Published: 2026-04-09

Production editor:
Ananya Mallik

Handling editor:
Sarah Lambart

Reviews:
Two anonymous reviewers

Copyediting:
Lan Luo
Elliot Carter
Marthe Klöcking

Planetary and geological melts and magmas produced at depth encounter rocks at a variety of temperatures and redox conditions during their ascension towards the surface of planetary bodies. Reactions occur between the magma and surrounding rock material, but despite their potential importance for the regulation of magmatic differentiation, the rates of such interactions are rarely considered and poorly known. The aim of this work is to review the results of high-temperature experiments and kinetic models for the dissolution of the main rock-forming minerals in aluminosilicate melts, that may be applied to partial melting of common rock types, and reactions between the melts and the principal rocks composing the lithosphere. A kinetic equation allowing the first-order prediction of mineral dissolution rates in planetary and geological melts was generated. The diffusion-controlled dissolution rate r (mol cm^{-2} s^{-1}) of common rock-forming silicate minerals in aluminosilicate melts at (1300 ± 20) °C and < 1 GPa pressure can be described by an inverse function of the viscosity of boundary layer melt (i.e. that formed at the crystal–melt interface upon the dissolution) independent of silicate mineral composition according to: $r = k\eta^{-n}$, where the correlation coefficient $k = 4 \times 10^{-7}$ mol cm^{-2} s^{n-1} Pa^n, $n = 0.5$, and η (Pa s) is the viscosity of the boundary layer melt (for $\eta \leq 1 \times 10^5$ Pa s). This function relating dissolution rate and melt viscosity is consistent with a simple detachment mechanism involving network-forming Si–O atoms during silicate mineral dissolution. This equation can be applied to the dissolution of the principal rock-forming minerals during melt–rock interactions in the lithosphere such as lithosphere assimilation. It shows that low-viscosity mafic–ultramafic magmas can be significantly more contaminated by lithosphere rock material compared to the high viscosity felsic magmas. This correlation for the main rock-forming minerals may be directly applicable to planetary lithosphere assimilation by magmas, magma mixing as well as the modeling of mantle metasomatism or other types of melt–rock interactions. Future efforts should be concentrated on developing kinetic models and providing further experimental constraints on the kinetic factors that control mineral–melt reactions in the terrestrial and planetary mantles.

1 Introduction

Crustal assimilation, anatexis, partial melting, mantle metasomatism, magma mixing and melt-mush interaction, are processes that all involve reactions between melts and minerals. Recently it has been recognized that magmatic differentiation in large crustal plutons may also be controlled by equilibration of melts with minerals in magmatic mushes (Jackson et al., 2018). However, such melt–rock and melt–mush interactions involving multiple reactions between minerals and melts cannot be modeled based exclusively on the concept of thermodynamic equilibrium (Zhang, 2013) but also involve kinetic effects (rates, mechanisms and timescales; e.g., Borisova et al., 2021a and references therein). Indeed, while the notion of thermodynamic equilibrium can be used to predict the direction of a chem-

ical reaction, it cannot inform about reaction rates or whether equilibrium will ever be reached (Zhang, 2008, 2013). Modeling of geologically relevant processes involving mineral dissolution thus requires the use of kinetic models whose parameters may be deduced from relevant mineral dissolution experiments (e.g., see Ghiorso, 1987).

Experiments on the kinetics of mineral dissolution in silicate melts have been performed for more than 50 years, initiated by researchers from the ceramics and glass-making communities (Cooper Jr, 1962; Cooper Jr and Kingery, 1964; Oishi et al., 1965; Scherer et al., 1970). Numerous experiments on the dissolution of the principal geologically relevant rock-forming minerals in silicate melts were subsequently performed in the 1980s (e.g., Kuo and Kirkpatrick, 1985a,b and references therein). However, despite the large amount of data available, no widely accepted kinetic model has yet been published. Kuo and Kirkpatrick (1985a) were the first to summarize experimental data on the dissolution of mafic minerals in basaltic melts available at that time in order to calculate the ascent velocities of peridotite xenolith-bearing basaltic magmas. The first attempt to construct a general and relatively simple kinetic model of crustal assimilation by magmas was performed by Edwards and Russell (1996, 1998) based on available experimental data on mineral dissolution and thermodynamic modeling of melt crystallization, but did not consider the factors controlling mineral dissolution rates. In addition to studies dedicated to mineral dissolution, numerous studies have experimentally investigated related and relevant topics, for example, the partial melting of crustal mineral assemblages such as quartz and phlogopite (e.g., Tsuchiyama and Takahashi, 1983; Tsuchiyama, 1985a,b; Pichavant et al., 1996; Hammouda et al., 1996; Hammouda and Pichavant, 1999) and quartz and felsic rock dissolution in silicate melts (Zhang et al., 1989; Liang, 1999; Shaw, 2000, 2004, 2006, 2012; London et al., 2012). Building on experimental data on melt–rock interaction, Liang (1999, 2003), Morgan et al. (2006), Chen and Zhang (2008, 2009) and Alexander (2011) developed kinetic models that could be applied to the principal geologically relevant silicate minerals. Moreover, using results of experiments on melt–peridotite interaction (e.g., Shaw et al., 1998; Shaw, 1999; Lundstrom, 2000; Morgan and Liang, 2003, 2005; Shaw and Dingwell, 2008; Van den Bleeken et al., 2010, 2011; Tursack and Liang, 2012; Wang et al., 2013, 2020; Borisova et al., 2020b, 2021a), models of crustal and mantle assimilation have been developed and applied to terrestrial basaltic magmatism and planetary felsic crust production (e.g., Borisova et al., 2017, 2020b, 2021a; Borisova, 2022). Other relevant efforts, such as modeling of diffusional processes in aluminosilicate melts, have been carried out in the nuclear industry (e.g., Pablo et al., 2019), industrial glass-making (e.g., Scherer et al., 1970; Claireaux et al., 2016; Yoshizawa et al., 2025) and material sciences (Bordère and Glockner, 2021). Advanced experimental and modeling approaches have been developed by the group of Y. Zhang since the publication on mineral dissolution in 1989 (e.g., Zhang et al., 1989; Chen and Zhang, 2008, 2009; Zhang, 2008, 2013; Yu et al., 2016, 2019). However, there has been no systematic study of the factors controlling diffusion-controlled mineral dissolution and the connection to melt viscosity, structure of the melt and the diffusion of network formers, in particular of boundary layer melts in contact with dissolving grains (in general it is the initial melt that is considered and not the one that results from dissolution).

In light of the existing corpus of experimental data, the aim of the present study is: i) to consider theoretical aspects and physical-chemical parameters controlling the kinetics of mineral dissolution; ii) to carry out a critical review of available models based on experimental dissolution of the main silicate rock-forming minerals and iii) to generate a kinetic equation allowing the first-order prediction of the dissolution rates of the rock-forming minerals (quartz, plagioclase, pyroxenes, and olivine) in geological and planetary melts at 1300 °C and 0.01 MPa to 1 GPa. Such a study is of interest for a better quantification of the rates of open-system process such as lithosphere (e.g., crustal) assimilation by magmas and magma hybridization, as well as for understanding the open-system reactions controlling the chemical and isotopic compositions of lavas and rocks observed on planetary surfaces.

2 Theoretical aspects of the solid–fluid and solid–melt interactions

2.1 The control of solid–fluid interactions

The main processes involved in the reactive transport of a fluid/melt through a porous and/or fractured solid media are illustrated in Figure 1. These include convection, molecular diffusion, mechanical dispersion and solid–fluid reactions (dissolution and crystallization). Crystal dissolution proceeds via the transport of dissolved reactants to the solid surface followed by their chemical reaction at the solid–fluid interface and the transport of the reaction products away from the interface. The overall crystal dissolution rate is controlled by the slowest step of these successive processes, either surface reaction or transport of species in the fluid/melt/solid (e.g., Berner, 1981; Lasaga, 1995; Zhang, 2013). When solid surface reactions are fast relative to diffusion in fluid/melt, dissolved species are enriched in the liquid near the interface with the grain. Concentrations in the liquid at the melt–grain interface can approach equilibrium with the solid grain and dissolution may be considered as "transport controlled" (Fig. 2a). In this case, the interface liquid composition is very close to that in equilibrium with the solid and its composition is thus different from the far-field liquid (Fig. 3) composition (Zhang, 2008, 2013). On the other hand, if transport in the melt is fast relative to surface reactions, very weak concentration gradients of the dissolved component occur in the fluid and the overall reaction rate is "surface reaction controlled" (Fig. 2b). In this case, the interface liquid composition is close to that of the far-field composition (Zhang, 2008, 2013). The rotating disk reactor method (Gregory and Riddiford, 1956) allows discrimination between transport

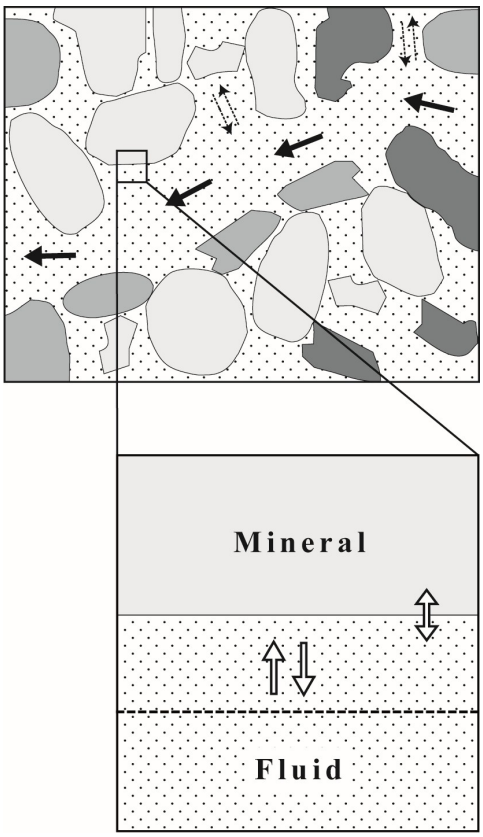

Figure 1. Schematic illustration of a mineral–fluid interface in a porous rock. Dissolved species can be transported by either convection or diffusion as shown by the solid and dashed arrows, respectively. The fluid adjacent to the mineral surface is immobile; transport of elements to and from the solid surface requires diffusion through this fluid boundary layer (after Schott et al., 2009).

and surface reaction control in aqueous fluids by changing the rotation speed of a solid disk subject to dissolution. It has been successfully applied to approximate the thickness δ_e of the diffuse boundary layer that forms between the solid surface and the convective fluid and thus to quantify the dissolution rate constants of fast reacting minerals like calcite (Alkattan et al., 1998) or basaltic glass (Guy and Schott, 1989). A similar design—a rotating cage with a crystal—was used by Watson (1982) to investigate dynamic quartz dissolution at 1300 °C and 1400 °C in a basaltic melt and to estimate both δ_e and quartz dissolution rate values.

Because the activation energy E_a for breaking bonds—the parameter that controls surface reaction—is much greater for most silicate minerals than activation energies for diffusion in a fluid ($E_a \sim 85$–335 versus < 20 kJ mol^{-1}; Lasaga, 1981), another way to discriminate between the transport and surface reaction controlled regimes is to quantify the apparent activation energy of crystal dissolution via experiments performed at different temperatures. This approach has been applied by Wagstaff (1969), Kuo and Kirkpatrick (1985a), Kerr (1995) to show that the dissolution close to equilibrium of diopside in diopsidic melt at ~ 1400 °C is controlled by chemical reaction at the melt–crystal interface but that the dissolution of the same crystal at far from equilibrium conditions is controlled by chemical diffusion in the silicate melt, a control that depends on the temperature.

2.2 Basics of kinetics and thermodynamics

2.2.1 Reaction rates

Most reactions involving silicate minerals in aqueous fluids and melts can occur in both the forward (dissolution) or backward (precipitation) directions. The net rate, r, of the overall reaction is the difference between the forward, r_+, and the backward, r_-, rates:

$$r = r_+ - r_- \tag{1}$$

The application of the principle of detailed balance or the Transition State Theory to any elementary reaction leads to the following expression of the overall rate (Lasaga, 1981; Aagaard and Helgeson, 1982; Schott et al., 2012):

$$r = r_+ \left(1 - e^{\Delta G/RT}\right) \tag{2}$$

where ΔG stands the free energy change for the considered reaction and R is the gas constant. Equation 2 ensures that the overall rate is equal to zero at equilibrium ($\Delta G = 0$) and implies that the backward reaction rate equals zero far from equilibrium ($\Delta G < \sim 3RT$). Near equilibrium, the magnitude of ΔG is small relative to T and Equation 2 can be simplified to $r = -\frac{r_+ \Delta G}{RT}$ which shows a linear relation between the overall rate and ΔG. It should be noted that non-linear rate laws of the form $f(\Delta G) = \left[1 - \exp(\Delta G/RT)\right]^n$ have been applied both for mineral dissolution and growth occurring at dislocations intersecting the crystal surface (Kirkpatrick, 1981; Burch et al., 1993; Shiraki and Brantley, 1995; Lasaga and Luttge, 2001). Finally, the forward rate can be expressed as:

$$r_+ = k_+ S_r \prod a_i^{n_i} \tag{3}$$

where k_+ stands for the dissolution rate constant, S_r represents the solid reactive surface area and $\prod a_i^{n_i}$ accounts for the catalysis or inhibition of the reaction by the activity of the ith aqueous/melted species/complex. The influence of temperature on k_+ is generally described by the classical Arrhenius equation:

$$k_+ = Ae^{-E_a/RT} \tag{4}$$

where A is the pre-exponential factor and E_a is the activation energy.

2.2.2 The Gibbs free energy of mixing of silicate melts

Using Equation 2 to describe the dissolution kinetics of a solid in silicate melts requires the quantification of the chemical affinity, $A = -\Delta G$ of the dissolution reaction or, as $\Delta G = RT \ln \Omega$, the value of the saturation state Ω of the melt with respect to the dissolving solid (Nagy and Lasaga, 1992). This implies the availability of thermodynamic models which quantify the relative stability of solid and liquid phases in igneous systems. If the thermodynamic

properties of the coexisting solids are known, then, in principle, the Gibbs free energy of the liquid may be derived from available experimental liquid–solid data. Adopting the thermodynamic database of Berman (1988) for rock-forming minerals and extending it to include consistent thermodynamic models for relevant igneous solid solutions, Ghiorso et al. (1983); Ghiorso (1985); Ghiorso and Sack (1995); and Ghiorso and Gualda (2015) have analyzed all available data on liquid–solid experiments to estimate the liquid mixing properties. This resulted in a regular solution-type thermodynamic model for twelve-components silicate liquids in the system SiO_2–TiO_2–Al_2O_3–Fe_2O_3–FeO–MnO–MgO–CaO–Na_2O–K_2O–P_2O_5–H_2O over the temperature range (900–1700 K) and pressures up to 4 GPa. The molar Gibbs free energy of natural silicate liquids ($\overline{G}$) can be defined by (Ghiorso et al., 1983; Ghiorso and Sack, 1995; Gualda et al., 2012)

$$\begin{aligned}\overline{G} = &\sum_{i=1}^{n} X_i \mu_i^0 + RT \sum_{i=1}^{n} X_i \ln X_i \\ &+ \frac{1}{2} \sum_{i=1}^{n} \sum_{j=1}^{n} W_{i,j} X_i X_j \\ &+ RT \left[X_w \ln X_w + (1 - X_w) \ln(1 - X_w) \right]\end{aligned} \tag{5}$$

where R is the gas constant, T is the absolute temperature (K), and $W_{i,j}$ are temperature, pressure-independent regular solution type interaction parameters. Optimal values of the $W_{i,j}$ parameters are derived by constraining compositional derivatives of $\overline{G}$ with experimental data on the compositions of silicate liquids.

The reaction of solid phase φ with the melt is described by Ghiorso and Sack (1995):

$$\varphi_p = \sum_{k=1}^{n} \vartheta_{p,k} c_k \tag{6}$$

where φ_p refers to the p^{th} end-member component of the phase of interest (for example, forsterite, Mg_2SiO_4, in olivine), c_k refers to the formula for the k^{th} component in the liquid, and $\vartheta_{p,k}$ to the stoichiometric reaction coefficient for the k^{th} liquid component. The law of mass action for Equation 5 yields:

$$\Delta G_{\varphi_p} = -A_{\varphi_p} = \Delta G^0_{\varphi_p} + \sum_{k=1}^{n} \vartheta_{p,k} \ln a_k - RT Ina_{\varphi_p} \tag{7}$$

Expanding and rearranging Equation 7 leads to

$$\begin{aligned}-\Delta G^{\circ}_{\varphi_p} - RT \sum_{k=1}^{n} \vartheta_{p,k} \left[\ln X_k + \ln(1 - X_w) \right] \\ = A_{\varphi_p} - RT \ln a_{\varphi_p} \\ + \sum_{i=1}^{n} \sum_{j=1}^{n} \left[\sum_{k=1}^{n} \left(\vartheta_{p,k} \delta_{k,i} X_i - \frac{1}{2} \vartheta_{p,k} X_i X_j \right) \right] W_{i,j}\end{aligned} \tag{8}$$

where the "unknowns" are summarized on the right-hand-side of the equation (Ghiorso and Sack, 1995).

2.2.3 *Diffusion control of crystal dissolution*

As illustrated by Figures 2 and 3, diffusion control of dissolution/crystallization occurs when the surface reaction kinetics is fast enough to ensure that the composition of the fluid or melt adjacent to the surface of the dissolving or growing crystal is in equilibrium with the solid. The rate of dissolution in this case may be determined from the transport equations. A simple example, the dissolution of a sphere of radius a in an unstirred fluid, was considered by Lasaga (1998). The concentration of the solute at $r = a$ adjacent to the sphere is the equilibrium value, C_{eq} whereas C_b is the concentration in the initial bulk fluid. The flux of solute away from the sphere surface is given by (Lasaga, 1998):

$$J = -D\left(\frac{\partial C}{\partial r}\right)_{r=a} = D\frac{a\left(C_{eq} - C_b\right)}{a^2} \tag{9}$$

Multiplying the flux J by the molar volume of the solute, $\overline{V}$, converts J to units of volume added (removed)/unit

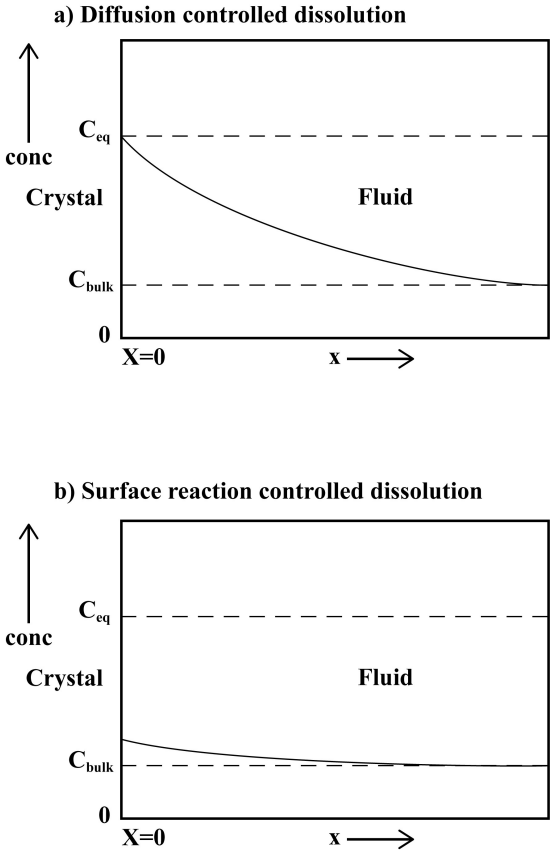

Figure 2. Evolution of the concentration of a crystal component as a function of the distance from the crystal surface during diffusion control (a) and surface reaction control (b) dissolution. Note that if the surface reaction is very fast, the reaction is diffusion controlled and the component concentration near the crystal surface is in equilibrium with the crystal.

surface area of sphere/unit time, which is the decrease (or increase) in the radius of the sphere:

$$\frac{da}{dt} = -\frac{\overline{V}D}{a}\left(C_{eq} - C_b\right) \tag{10}$$

Equation 10 is often referred to the diffusion controlled reaction rate for a sphere. If $a \sim a_0$ for $t = 0$, Equation 10 can be integrated to:

$$a_0 - a = \sqrt{2D\overline{V}\left(C_{eq} - C_b\right)t} \tag{11}$$

The dependence of $a_0 - a$ on the square root of time is typical of a diffusion-controlled process. For crystals composed of several atomic species, which is the case of most minerals, several components must be considered when modeling chemical equilibrium. Considering a crystal of type "AB" (i.e. NaCl or Mg_2SiO_4), the equilibrium condition is $C^A_{eq}C^B_{eq} = K_{eq}$, where K_{eq} is the effective mineral solubility product (i.e. it includes the activity coefficients of dissolved species A and B). In addition, assuming stoichiometric dissolution of the crystal, the diffusion fluxes of A and B at the crystal surface must be equal ($J_A = J_B$). A similar result is obtained if reaction is limited by diffusion through a boundary layer of thickness L next to the surface of the dissolving crystal. In this case the diffusion flux is given by

$$J_A = D_A\frac{C^A_{eq} - C^A_b}{L} = J_B = D_B\frac{C^B_{eq} - C^B_b}{L} \tag{12}$$

The expressions of C^A_{eq} and C^B_{eq} have been given by Lasaga (1998) and the dissolution rate (or growth) of the spherical crystal is expressed as (Lasaga, 1998):

$$\begin{aligned}\frac{da}{dt} = \frac{\overline{V}}{2a}\Bigg[&\left(D_AC^A_b + D_BC^B_b\right)\\ &-\Bigg[(D_AC^A_b + D_BC^B_b)^2\\ &-4\left(C^A_bC^B_b - K_{eq}\right)D_AD_B\Bigg]^{1/2}\Bigg]\end{aligned} \tag{13}$$

Note that if $C^A_b = C^B_b = C$ and $D_A = D_B = D$, diffusion coefficients, then Equation 13 simplifies to

$$\frac{da}{dt} = \frac{\overline{V}D}{a}\left(C - \sqrt{K_{eq}}\right) \tag{14}$$

which is the normal diffusion-controlled rate law for one component except that C_{eq} is replaced by the solubility product K_{eq}.

If the diffusion rate law is proportional to the concentration difference, the dependence of the net rate on the chemical affinity (A) for systems involving several components is not as simple. Given values of C^A_b and C^B_b, A can be calculated from

$$A = -RTln(\frac{C^A_bC^B_b}{K_{eq}}) \tag{15}$$

Using calculated values of C^A_{eq} and C^B_{eq}, a plot of the rate of diffusion-control dissolution can be calculated as a function of ΔG using Equations 10 and 15. Figure 4 illustrates the variation of the rate of crystal dissolution as a function of the departure from equilibrium (i.e. $-\Delta G/RT$) using dimensionless values equal to unity of L, D_A, D_B and K_{eq}, and allowing C_A and C_B to vary such that $C_A = C_B$. This figure clearly shows that the diffusion-controlled dissolution (or growth) rate of multicomponent crystals is a non-linear function of the departure from equilibrium.

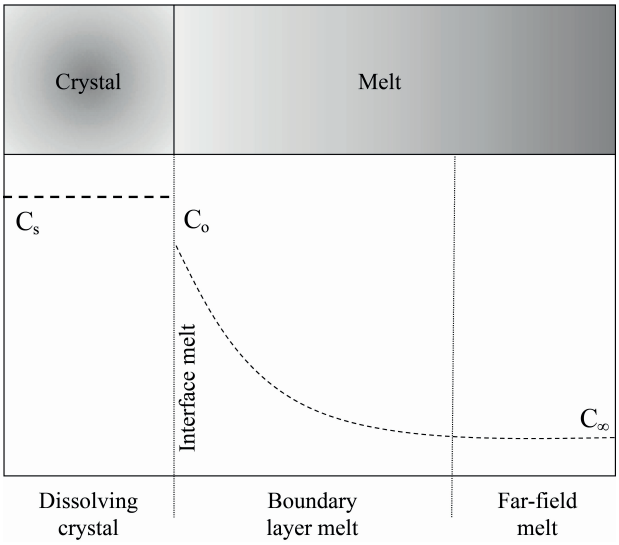

Figure 3. Concentration (C) of a given species as a function of the distance from the crystal–melt interface during diffusion-controlled dissolution of a silicate mineral crystal with formation of the boundary layer melt. Upon the dissolution of the crystal in the silicate melt, the boundary layer, is developed characterized by the characteristic interface melt and the far-field melt. C_s, C_o and C_∞ correspond to the concentrations in the crystal, in the interface melt (saturation or equilibrium content in the melt) and in the far-field melt, respectively. The transport control of dissolution rate by diffusion causes the interface melt to be in equilibrium with the crystal (e.g., Oishi et al., 1965; Zhang, 2008). At infinity, the far-field melt composition is independent of time.

Values of diffusion coefficients can vary by many orders of magnitude, as illustrated in Figure 5 where Ar diffusion data in air, water, silicate melts and solid hornblende are reported. It can be seen that typical values of Ar diffusion coefficients are very high in air (about $10^{-5}\,m^2\,s^{-1}$ at 25 °C), intermediate in water (about $10^{-9}\,m^2\,s^{-1}$ at 25 °C) and much smaller in aluminosilicate melts (about 10^{-13} to $10^{-15}\,m^2\,s^{-1}$ at 800 °C) and in hornblende (about $10^{-18}\,m^2\,s^{-1}$ at 800 °C). For this reason, mineral–melt interactions are more often controlled by diffusion than mineral-aqueous solution interactions. From one species to another, diffusion in an aqueous liquid or an aluminosilicate melt depends on the bond strength as well on the size of the diffusing species, which in turn depend on concentration and liquid/melt composition (Zhang, 2010). Below the important parameters controlling diffusivities are briefly reviewed.

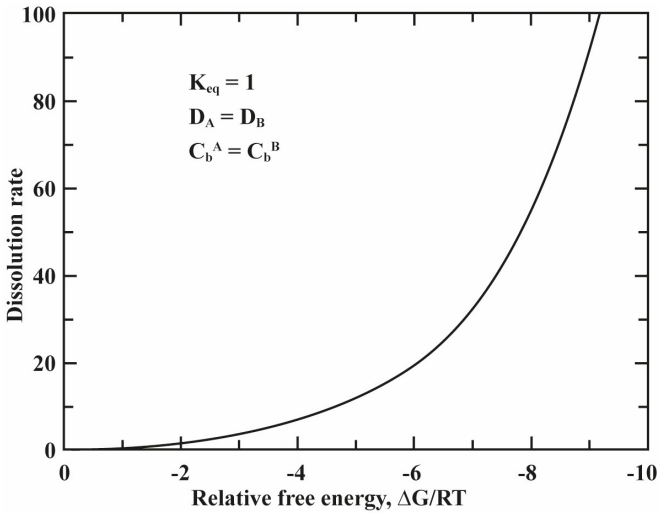

Figure 4. Plot of diffusion controlled dissolution rate of a mineral AB as a function of departure from equilibrium ($-\Delta G/RT$). Rate is in dimensionless units. Both C_b^A and C_b^B are allowed to vary such that $C_b^A = C_b^B$. Note that the rate is nonlinear in ΔG (modified after Lasaga, 1998).

The temperature dependence of diffusivities is described by the well-known Arrhenius equation

$$D = D_0 e^{-E^*/RT} \tag{16}$$

where D_0 stands for the pre-exponential factor and E^* is the activation energy. Equation 16 predicts that plots of $\ln D$ versus $1/T$ are straight lines. Deviation from straight lines may indicate a change in the diffusion mechanisms. Values for E^* range from a few kJ/mol for ions in aqueous solution to several hundred kJ/mol for ionic diffusion in silicate melts and minerals. Of particular interest is the so-called diffusion compensation law, which predicts a linear relationship between E^* and $\log D_0$ (see examples in Lasaga, 1998).

The effect of pressure on the diffusion coefficient depends on the activation volume ΔV^* for diffusion according to:

$$D = D_0 e^{-E^*/RT} e^{-P\Delta V^*/RT} \tag{17}$$

At 800 °C, with a ΔV^* of 5 $cm^3\,mol^{-1}$, Equation 17 predicts that the diffusion coefficient is divided by 1.8 and 270 when the pressure is increased from 1 bar to 1 and 10 kbar, respectively. Note that the activation volume does not have to be positive. For example, the oxygen diffusion coefficient in SiO_2 melts increases with pressure up to 10 GPa (Kubicki and Lasaga, 1991).

The impact of the concentration of a given species A in the fluid/melt on its diffusion coefficient can be derived from the Nernst-Einstein equation and Fick's first law (Lasaga, 1998):

$$D_A = D_A^0 \left(1 + \frac{\partial ln\gamma_A}{\partial lnC_A}\right) \tag{18}$$

The term in brackets is called the thermodynamic term with γ_A and C_A standing for the activity coefficient and concentration of A, respectively. The term D_A^0 is the diffusion coefficient of A at infinite dilution. Equation 18 illustrates the effects of non-ideality on the diffusion coefficient. For example, in the case of dilute electrolyte solutions obeying the Debye-Hückel theory, γ_A varies as $\sqrt{C_A}$.

The viscosity of the fluid/melt is another variable that affect the diffusion coefficient. Two equations can been used to describe the diffusion coefficient. The Stokes-Einstein equation:

$$D = \frac{k_B\ T}{6\pi\eta\ r*} \tag{19}$$

and Eyring equation:

$$D = \frac{k_B T}{\eta\lambda} \tag{20}$$

In these equations, η stands for the viscosity of the fluid (in Pa s), k_B is Boltzmann's constant ($m^2\,kg\,s^{-2}\,K^{-1}$), T is the absolute temperature (K) and r^* is the radius of the diffusing species (Å) in the Stokes-Einstein equation, whereas D is the self-diffusivity of a single component present, and λ is the characteristic particle translation distance (Å) in the Eyring equation (Eyring, 1935). The Stokes-Einstein equation yields reasonable values for D in aqueous solutions but it has been found to poorly approximate diffusion coefficients of small ions in silicate melts. The Eyring relation predicts an inverse relation between the diffusion coefficient and viscosity uniquely for network formers such as Si and Al in silicate melts (Dingwell and Webb, 1990; Mungall, 2002). While it appears to work for Si self diffusion in silicate melts (Lesher et al., 1996; Mungall, 2002), it does not work for ^{18}O diffusion in the melts (Dunn, 1982; Zhang, 2010). This can be related to bulk oxygen diffusion controlled by physically dissolved oxygen in the melt (Dingwell and Webb, 1990).

2.2.4 *Multicomponent diffusion in silicate melts*

The movement of a mineral during the dissolution process is related to the Rayleigh instability that may create convection-controlled dissolution (mostly in mafic and ultramafic systems), whereas dissolution (mostly in felsic and intermediate melts) without any motion related to convection is purely diffusion-controlled (Zhang, 2013). Multicomponent chemical diffusion in aluminosilicate melts originates in the gradients of the chemical potentials of the melt components. Multicomponent diffusion is likely the primary but not unique process controlling mineral dissolution and growth in silicate melts. Modeling of multicomponent diffusion and diffusion-controlled dissolution of minerals advances our knowledge of the kinetics of mineral dissolution and growth with the development of experimental methods and the application of diffusion matrices (Chakraborty et al., 1995a,b; Zhang, 2008). Pioneering works on the diffusion matrix application to geologically relevant melts were those of Trial and Spera (1994) who proposed an optimized experimental strategy for the calculation of diffusion coefficients, and those of Chakraborty et al. (1995a,b) who demonstrated the utility of eigenvalues and eigenvectors (eigenvalues and eigenvectors are the main parameters of

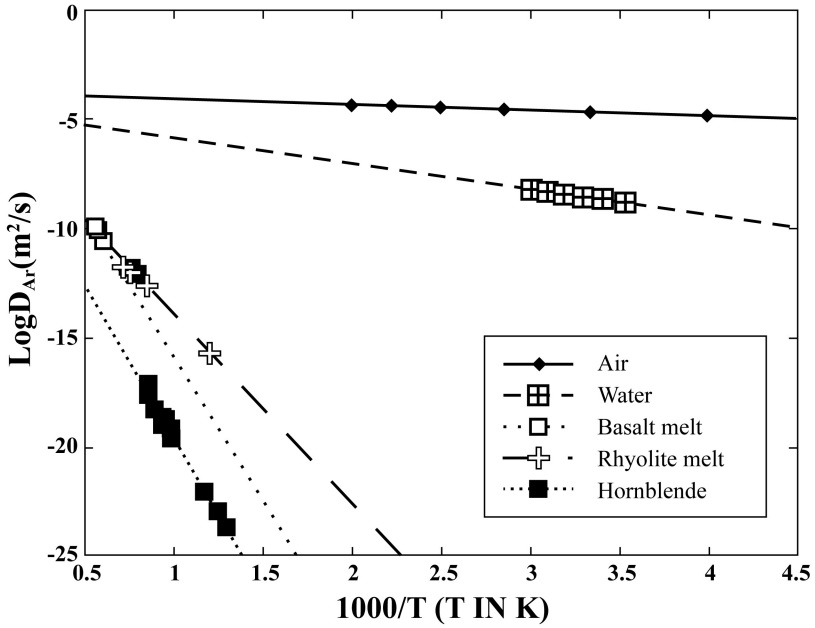

Figure 5. Molecular diffusion coefficient of argon (Ar) in air (gas) (in m^2 s^{-1}) calculated using equations in Cussler (1997), water (Wise and Houghton, 1966), basalt melt (Nowak et al., 2004), rhyolite melt (Behrens and Zhang, 2001) and hornblende (Harrison, 1982) as a function of reciprocal (in K). The figure is modified after Zhang (2010).

mathematical matrix in linear algebra, see below) of the diffusion matrix. The eigenvalues are independent of the choice of components, whereas the numerical values of the eigenvectors change depending on the choice of components used to describe the melt composition (Chakraborty et al., 1995b; Zhang and Gan, 2022). Today, diffusion-controlled dissolution may be modeled through either the use of effective binary diffusion coefficients or the diffusion D matrix (Claireaux et al., 2016; Shaw et al., 2018; Pablo et al., 2019; Guo and Zhang, 2020; Zhang and Gan, 2022). In an n component system, the expanded Fick's law for one-dimensional diffusion takes the following form:

$$J_1 = -D_{11}\frac{\partial C_1}{\partial x} - D_{12}\frac{\partial C_2}{\partial x} - \cdots - D_{1n}\frac{\partial C_n}{\partial x} \quad (21)$$

$$J_2 = -D_{21}\frac{\partial C_1}{\partial x} - D_{22}\frac{\partial C_2}{\partial x} - \cdots - D_{2n}\frac{\partial C_n}{\partial x} \quad (22)$$

$$J_n = -D_{n1}\frac{\partial C_1}{\partial x} - D_{n2}\frac{\partial C_2}{\partial x} - \cdots - D_{nn}\frac{\partial C_n}{\partial x} \quad (23)$$

$$\begin{pmatrix} J_1 \\ J_2 \\ \vdots \\ J_n \end{pmatrix} = -\begin{pmatrix} D_{11} & \cdots & D_{1n} \\ \vdots & \ddots & \vdots \\ D_{n1} & \cdots & D_{nn} \end{pmatrix} \begin{pmatrix} \frac{\partial C_1}{\partial x} \\ \frac{\partial C_2}{\partial x} \\ \vdots \\ \frac{\partial C_n}{\partial x} \end{pmatrix} = -\mathbf{D}\frac{\partial}{\partial x}\begin{pmatrix} C_1 \\ C_2 \\ \vdots \\ C_n \end{pmatrix} \quad (24)$$

The diffusion equations can be solved by the diagonalization of **D** using eigenvalues and eigenvectors:

$$\mathbf{D} = \mathbf{P}\,\Lambda\,\mathbf{P}^{-1} \quad (25)$$

where Λ is a diagonal matrix whose diagonal elements λ_i are the eigenvalues of **D**, and **P** is the eigenvector matrix, with column j corresponding to the eigenvalue λ_j (Zhang and Gan, 2022).

As an example, the experimental data of Shaw et al. (2018) demonstrated that the dissolution of sapphire (Al_2O_3) in a $Ca-Al_2O_3-SiO_2$ (CAS) melt is diffusion-controlled and a function of the diffusion of Al_{xs} (i.e., the Al that is not charge balanced by Ca, a species that diffuses even slower than Si in this case). Guo and Zhang (2020) also applied the diffusion matrix to basaltic systems and demonstrated that the two slowest eigenvectors involve exchange of Si and/or Al with non-alkalis. Finally, Claireaux et al. (2016) demonstrated that in the Na-bearing CNAS (Ca–Na–Al–Si) system, the eigenvector corresponding to the exchange of Ca with Si and Al was the slowest. The authors interpreted the eigenvectors as simple local exchanges between the considered atoms. More factors controlling the mineral dissolution in silicate melts are considered below.

3 Review of kinetic models of mineral dissolution

3.1 Early kinetic models

Tsuchiyama (1986) was one of the first to find that diffusion of chemical elements in the solid plays an important role in the melting and dissolution of crystalline solid solutions. Zhang et al. (1989) conducted experimental dissolution of olivine, diopside, spinel, quartz and rutile in andesite melts at 1215–1400 °C and 0.5–2.2 GPa, and observed that the dissolution of these minerals was controlled by diffusion. Much later, Y. Zhang's group performed similar piston-cylinder experiments at variable pressures (e.g., Zhang

et al., 1989; Zhang, 2008; Chen and Zhang, 2008, 2009; Zhang, 2013; Yu et al., 2016, 2019). These authors noticed that all previous work, with the exception of Harrison and Watson (1983), Watson and Harrison (1984) and Watson and Jurewicz (1984), investigated mineral dissolution in runs where convection operated in the melt. Zhang et al. (1989) proposed a model of mineral dissolution based on three possible rate-controlling mechanisms: surface reaction, diffusion, and convection. For this purpose, they expressed the interface reaction rate as a function of the degree of saturation of the melt with respect to the mineral phase. Their equations for the diffusion reaction were based on two assumptions: i) a dependence on the degree of undersaturation, b (or Θ) $= \frac{C_o - C_\infty}{C_s - C_o}$, of the melt composition and ii) diffusion in the melt, treated as binary diffusion (D), using an effective binary diffusion coefficient, EBDC (e.g., Zhang et al., 1989; Liang et al., 1996; Shaw, 2012; Zhang and Xu, 2016). Zhang et al. (1989) suggested the following order of mineral dissolution rates in andesitic melt: orthopyroxene, clinopyroxene, plagioclase > olivine, spinel > accessory minerals (apatite and zircon, etc.). Zhang et al. (1989) proposed an equation for the convection-driven control of dissolution:

$$r = \frac{D}{\delta}\frac{C_o - C_\infty}{C_s - C_o} = b\frac{D}{\delta} \tag{26}$$

Numerous authors have used the b (or Θ) parameter, where r is the mineral dissolution rate, δ stands for the boundary layer thickness, and D is the diffusion coefficient and following parameter based on the degree of undersaturation of melt with a mineral phase. The equation of the degree of undersaturation was used by many authors thereafter (e.g., Kerr, 1995; Morgan et al., 2006; Chen and Zhang, 2008, 2009). In summary, these authors found that the role of the crystal–melt interface was relatively unimportant in the control of dissolution rate but it could become significant when the dissolution temperature was close to the liquidus temperature of the dissolving crystal. Nevertheless, surface reaction is dominant at low temperature in highly supercooled aluminosilicate liquids, as illustrated by Roskosz et al. (2005, 2006). Zhang et al. (1989) emphasized that diffusion was the major rate-controlling factor for mineral dissolution in silicate melts.

Donaldson (1985) and Kuo and Kirkpatrick (1985a) summarized the results of the first experiments on the dissolution of silicate minerals (olivine, clinopyroxene, orthopyroxene, plagioclase, quartz, garnet) in basaltic, andesitic and rhyolitic melts. Donaldson (1985, 1990) noticed that the dissolution rate of quartz as a function of temperature follows an Arrhenius relation. Based on the derived value of the activation energy ($E^* \sim 167$ kJ/mol), Donaldson concluded that dissolution was controlled by diffusion rather than surface reaction. However, the measured values of quartz, plagioclase, pyroxene, and olivine dissolution rates in basaltic melt at a given temperature may have been affected by relative movements of solid and liquid during the experiments (i.e. convection), such that a diffuse boundary layer, through which matter is transferred, develops between the solid surface and the homogeneous bulk fluid. At steady-state, the surface reaction and transport fluxes are equal resulting in a time-independent crystal dissolution rate. For example, time-independent dissolution rate of a quartz sphere in a basaltic melt (Watson, 1982) is indicative of quartz convection-controlled dissolution through a diffuse (boundary) layer.

Detailed investigation of olivine dissolution in basaltic melt has been performed by Thornber and Huebner (1982) to better understand the origin of lunar basaltic glasses. These authors show that olivine dissolution rate was independent of the crystal face in contact with the solution. They also noticed that the dissolution rate increases with temperature. Another conclusion was that the rates of the partial dissolution or resorption of olivine are greater in more siliceous melt (richer in SiO_2 content). The latter conclusion may be related to incongruent dissolution of olivine in the Si-rich system and may depend on the melt composition. Kuo and Kirkpatrick (1985a) found that in the diopside-forsterite-silica system the melt composition at the interface frequently reflects near-equilibrium with respect to the solid. The composition of the melt at the interface remains constant if the system is semi-infinite. Analyzing their experimental data on peridotite dissolution in basaltic melts, Kuo and Kirkpatrick (1985a) noticed that the dissolution rate of garnet was the fastest among the peridotite-hosted minerals. These authors also indicated that silicate mineral dissolution may be controlled by both diffusion and convection. For example, during time-independent dissolution rates, identical concentration gradients at the boundary layer for the same mineral phase and the linear correlation between dissolution rate and apparent diffusion coefficients indicate the coupled roles of diffusion-controlled dissolution and convection.

Based on high pressure experiments and available literature data at 1.3–2.0 GPa, Scarfe et al. (1980) and Kuo and Kirkpatrick (1985a) found that the dissolution rate of silicate minerals decreases with increasing pressure. To assess magma ascent velocities, the authors proposed that the dissolution rate of a xenolith can be described by that of olivine because olivine is the most abundant mineral in peridotites. Compilation of experimental data on olivine dissolution rates allowed these authors to establish that the ascent velocities of alkali basaltic magmas could reach ~10 km/h.

3.2 Kinetic model of Edwards and Russell (1996, 1998)

Edwards and Russell (1996, 1998) carried out the broadest review of the dissolution rate experiments available before 1996. They built an empirical model of mineral dissolution rates based on available data for the main rock-forming minerals (olivine, orthopyroxene, clinopyroxene, spinel, garnet, quartz, alkali feldspar, plagioclase, and accessories zircon, apatite and rutile) in which the dissolution rates depend only on the reaction chemical affinity. Edwards and Russell (1996) applied normalization of the dissolution rates to the molar volume and the number of oxygen atoms in the mineral formula to provide dissolution rates expressed in o.e.m. $cm^{-2}\,s^{-1}$ (oxygen equivalent moles).

The proposed equations relate the normalized dissolution rates (r, mol cm^{-2} s^{-1}) to the calculated chemical affinity of the reaction of dissolution of the mineral in the melt according to:

$$r\,(\mathrm{mol\,cm^{-2}\,s^{-1}}) = 7.68\times10^{-11}A\,(\mathrm{J\,mol^{-1}}) + 5.27\times10^{-8} \quad (27)$$

where A is chemical affinity calculated as:

$$A = \sum_{j=1}^{m}\alpha(j,s)\mu(j,s) - \sum_{i=1}^{n}\alpha(i,m)\mu(i,m) \quad (28)$$

In this equation, $\alpha(j,s)$ and $\alpha(i,m)$ are stoichiometric reaction coefficients in moles for the j^{th} and i^{th} components in the solid (s) and melt (m) phases, respectively, and $\mu(i,m)$ denotes the chemical potential at the temperature (T) and pressure (P) of interest.

The values of A, chemical affinity, for a given mineral–melt reaction can be calculated using the standard state thermodynamic properties for solids from Berman (1988) and the corresponding thermodynamic code of Ghiorso and Sack (1995) using the composition of the starting melt at given values of temperature and pressure. Rhyolite-MELTS ($<$ 1 GPa pressure, Gualda and Ghiorso 2014) and related software (e.g., pMELTS, $\geq$ 1 GPa pressure) provide values of A for a limited set of mineral end-members at specified values of temperature, pressure and silicate melt composition. The parameters for chemical affinity, A, were calculated by these authors for the starting melt composition, because the evolution of the melt composition with time was not available. Relating experimental dissolution rates uniquely to the starting melt chemical composition and reaction affinity is an oversimplification. Indeed, the advancement of the dissolution reaction induces a change in melt properties (density, viscosity, composition, diffusion coefficient) and thus in the chemical affinity difference that affects dissolution rate. However, the principal equation (Eq. 27) does not ensure that the overall rate at equilibrium ($A = 0$) is equal to zero. Additionally, Edwards and Russell (1996) have also demonstrated that Arrhenius plots between $\ln(r)$ and $1/T$ (where T is the temperature) and A/RT (where A is the chemical affinity) can be used for modeling, suggesting that the affinity A allowed prediction of dissolution rate for, at least, superliquidus melt conditions. The authors' compilation of dissolution rates for the main silicate, oxide and phosphate minerals shows the following order for mineral dissolution in basaltic melts (of different composition): garnet $\geq$ plagioclase, olivine, clinopyroxene, orthopyroxene $\geq$ spinel (see Tables S1–S10, in the supporting dataset of Borisova, 2026). This order may be erroneous because the authors compiled all available mineral dissolution rates without taking into consideration pressure effects. Additionally, they used average mineral dissolution rates. In fact, this averaging strongly affects the calculated rate of mineral dissolution (e.g., $\sim 300\times10^{-7}$ cm s^{-1} for garnet) compared to the measured dissolution rates ($\sim$ 15 to 45×10^{-7} cm s^{-1}) at 1300 °C. The proposed order cannot be assumed to hold for all aluminosilicate melts because the dissolution rate is a complex function of the physical-chemical conditions, the melt-to-rock ratios and the melt composition in a given magmatic system.

3.3 Kinetic models of Liang (1999, 2000, 2003), Morgan et al. (2006) and Wang et al (2020)

To model quartz dissolution in the CAS ($CaO-Al_2O_3-SiO_2$) melt, Liang (1999, 2003) has considered the effect of chemical diffusion. For example, the flux of silica was found to be strongly coupled to the concentration gradients of CaO, MgO, K_2O in the natural melts of andesitic to rhyolitic composition (Liang, 1999 and references therein). Liang (1999) showed rapid attainment of diffusion control for quartz (and quartzite) dissolution in melts in the $CaO-Al_2O_3-SiO_2$ (CAS) system and stated that their model was applicable to haplodacitic and haplobasaltic melts. Liang (2003) demonstrated that in the absence of relative movement of crystals and liquid, crystal–melt re-equilibration was controlled by diffusion, dissolution and reprecipitation. Two regimes of crystal–melt re-equilibration were distinguished: controlled by diffusion-in-melt dissolution and controlled by diffusion-in-solid reprecipitation (Liang, 2000). This author also used the b (or Θ) parameter describing the degree of undersaturation of the melt with a mineral phase (but often omitted the units, a fact that complicates the task of using the models). Later, Morgan et al. (2006) demonstrated that the dissolution distance of anorthosite (Ca plagioclase) samples in picritic melt at 0.6 GPa and 1250–1400 °C is a linear function of the square root of time, consistent with a control of dissolution by the diffusion of anorthosite major constituents. This conclusion was confirmed by a plot of the anorthosite dissolution rate as a function of the reciprocal temperature which yielded an activation energy comparable to that for the self-diffusion of Si, Ca and Mg in a diopside melt. To model the dissolution process, these authors have expanded the EBDC by introducing an effective diffusion matrix, assuming diffusive coupling of SiO_2, Al_2O_3 and TiO_2 with the concentration gradients of CaO and FeO. Morgan et al. (2006) suggested that picritic magmas are capable of assimilating a significant amount of anorthosite material (the process of crustal assimilation in application to the Moon). These authors have also used the b (or Θ) parameter. A quantitative model of the formation of a compositional boundary layer around a xenolith during convective dissolution was developed by Wang et al. (2020). The consideration of this model is out of the scope of this review.

3.4 Kinetic models of Shaw (2000) to Shaw (2018)

At the same time, Shaw (2000) pointed out that the density contrast, generated in the melt near the crystal surface by crystal dissolution, results in a gravitational instability when the less dense melt layer is at the bottom of the experimental capsule. The density contrast between the interface melt and far-field melt is an efficient driving force for convection. Such convection prevents accurate characterization

of dissolution mechanisms and rates. Shaw (2004) also investigated the dependence of quartz dissolution rate on the crystal geometry and its localization in the experimental charge. He suggested that quartz dissolution was controlled by the chemical reaction at the crystal surface and found that the spherical geometry was not ideal for investigating the rates of mineral dissolution. Additionally, Shaw et al. (2018) investigated Al_2O_3 (sapphire) cylinder dissolution in CAS melts ($CaO-Al_2O_3-SiO_2$ system) and demonstrated that the dissolution rate decreases with increasing silica activity, viscosity and molar Al_2O_3/CaO in the melt.

In addition, Van Orman and Grove (2000) investigated clinopyroxene-ilmenite mineral pair dissolution in ultramafic glasses. The experiments performed at 0.1 MPa and 1.3 GPa (1050–1350 °C) constrain the phase equilibrium as well as the dissolution kinetics for the investigated minerals. The linear dependence between the diopside and ilmenite dissolution distances on the square root of the run duration indicated that the dissolution was controlled by diffusion. The results were interpreted in terms of the effective binary diffusion coefficient (D) obtained from fits of the SiO_2, TiO_2, Al_2O_3 and MgO concentration profiles ($C(x,t)$) using the diffusion equation from Zhang et al. (1989):

$$C(x,t) = C_\infty + \frac{(C_o - C_\infty)}{\mathrm{erfc}(-a)}\,\mathrm{erfc}\left(\frac{x}{2\sqrt{Dt}} - a\right) \tag{29}$$

where a is a parameter in the following expression:

$$\frac{C_o - C_\infty}{C_s - C_o} = \sqrt{\pi} a e^{a^2}\,\mathrm{erfc}(-a) \tag{30}$$

The authors mentioned that the smaller the compositional difference between the mineral and interface melt, the faster the dissolution rate. However, the calculation of the term of C_o in the interface (boundary layer) melt is impossible using the thermodynamic MELTS software because the kinetic run conditions are super-liquidus for the melt. The only information concerning mineral saturation at super-liquidus conditions can be extracted from the kinetic experimental runs through chemical analysis of the mineral–melt interface.

3.5 Kinetic models of Chen and Zhang (2008, 2009) and Guo and Zhang (2020) and related models

The theory of convective crystal dissolution has been initially developed by Kerr (1995), Zhang and Xu (2003) and finally applied by Chen and Zhang (2008, 2009) for crystal convective dissolution. The crystal convective dissolution (u) is a function of the thermodynamic, kinetic and fluid dynamics parameters of the system under consideration.

$$u = \frac{\beta D}{\delta} \tag{31}$$

$$\beta = \frac{\rho(C_o - C_\infty)}{\rho_s(C_s - C_o)} \tag{32}$$

where β is the dimensionless ratio of two concentration differences between the melt at the interface (C_o) and far-field melt (C_∞) and between the crystal (C_s) and (C_o) (Fig. 3). D is a diffusion coefficient related to the mass transport rate in the boundary layer; δ, the thickness of the boundary layer may be described by fluid dynamics (Chen and Zhang, 2009). These authors indicated that D/δ represents the transport rate constant and depends on temperature and pressure (e.g., Kerr, 1995). Kerr (1995) theoretically and experimentally investigated the effect of free and forced convection on crystal dissolution. His model predicts that partial melting and the destabilization and dissolution of large xenoliths and xenocrysts can strongly affect the reacting magma composition.

Chen and Zhang (2008, 2009) investigated the convective and diffusive dissolution of olivine and clinopyroxene in basaltic melts. They performed time-series experiments to characterize how the solid–melt interface evolves with time. The same equations as those of Zhang et al. (1989) describing the component concentration C as a function of the effective binary diffusivity of a component (D) in the melt were used.

The crystal dissolution distance, L, is given by:

$$L = 2\alpha\frac{\rho_m}{\rho_c}\sqrt{Dt} \tag{33}$$

where ρ_m and ρ_c are the density of the melt and crystal, respectively. Additionally, model equations for the convective mechanism were developed by the authors. According to Chen and Zhang (2008, 2009), the constant far-field melt composition must be verified in order to correctly interpret the compositional profiles and their potential control by diffusion. The melt at the interface may not be at saturation with the mineral phase, but the constancy of the interface melt composition as a function of time demonstrates that the dissolution rate is transport controlled. For example, Zhang et al. (1989) claimed that clinopyroxene reached 99 % of equilibrium within < 0.2 s of dissolution.

The diffusion-driven model of Guo and Zhang (2020) applied multicomponent diffusion to the modeling of olivine and anorthite dissolution in basaltic melts as well as to melt mixing (which happened in the Bushveld igneous complex during its formation). The authors noted that the model does not permit an accurate treatment of the temperature dependence of the diffusion matrix in basaltic system. They assumed, nevertheless, that the eigenvector matrix was constant with eigenvalues depending on temperature for successful modeling of the diffusion coefficients. Further development of diffusion studies therefore requires better understanding of the temperature dependence of the diffusion matrix in different magmatic systems.

Zhang Y. and collaborators (Zhang et al., 1989; Zhang, 2008, 2013) have established the general equation for dissolution rate using the effective binary diffusion approach:

$$\begin{aligned} -\frac{dr}{dt} &= \frac{\rho_{melt}}{\rho_{cryst}}\left(\frac{D}{\delta}\right)\frac{C_o - C_\infty}{C_{cryst} - C_o} \\ &= \frac{\rho_{melt}}{\rho_{cryst}}\left(\frac{D}{2a}Sh\right)\frac{C_o - C_\infty}{C_{cryst} - C_o} \end{aligned} \tag{34}$$

where $-\frac{dr}{dt}$ stands for the dissolution rate, δ is the average thickness of the boundary layer, ρ is the density, Sh is

the Sherwood number defined as $\frac{2a}{\delta}$, C_{cryst} (or C_s) is the concentration in the crystal, C_o is the concentration at the melt interface and C_∞ is the far-field melt concentration.

To summarize, most investigated mineral dissolution reactions in silicate melts at far from equilibrium conditions are controlled by transport (diffusion and/or convection) and not by chemical reactions at the crystal–melt interface. In contrast, the dissolution of diopside in diopside melts (Kuo and Kirkpatrick, 1985a) and the dissolution of mineral phases enriched in silica and alumina (e.g., quartz, sapphire, and corundum) may be controlled by chemical reactions at the crystal–melt interface.

In a little more detail, several factors discussed above and illustrated in Figure 6 can control mineral dissolution (which can be treated similarly to growth of a single crystal) in silicate melts. (a) The rate may be uniquely controlled by interface reaction (Fig. 6a) provided other parameters are constant. In this case, the profile is linear, the concentration gradient is absent and stirring would not affect the dissolution rate. (b) In the case of diffusion-controlled dissolution, the dissolution distance is proportional to the square root of time, a concentration gradient develops with time and the interface concentration is near equilibrium with respect to the melt, at least in semi-infinite system (Fig. 6b). (c) If convective mass transfer controls dissolution rate, the rate is independent of time, a concentration gradient appears in the melt and stays the same during the whole experiment, whereas the interface concentration is near saturation with respect to the melt (Fig. 6c). (d) Finally, if the rate is controlled by both reaction at the interface and diffusion of melt components, (Fig. 6d), a concentration gradient develops with time and the interface concentration progressively approaches saturation with respect to the solid.

3.6 Kinetic model of Alexander (2011)

The model of Alexander (2011) is based on the hypothesis that the mineral dissolution rate depends on the mechanisms occurring at the crystal–melt interface and also on melt diffusivities. The dissolution rate of such silicate minerals as olivine, clinopyroxene, and anorthite was thus assumed to be controlled by the thermodynamic and physical (structural) properties of the melt as well as the diffusional transport (self-diffusion of elements). Alexander (2011) proposed the following equations to describe the crystal dissolution rate:

$$\frac{dR_c}{dt} = -\frac{BT}{\eta}\left(1 - e^{A/RT}\right) \tag{35}$$

$$B = \frac{f k_B}{3\pi a_o^2} \tag{36}$$

where R_c is the crystal thickness (m), t is time (s), T is temperature (K), η is the viscosity (N m^{-2} s) of the melt at the crystal–melt interface, R is the gas constant (J mol^{-1} K^{-1}) and A is the chemical affinity. The parameter B is a function of the fraction, f, of the mineral surface sites available for attachment/detachment, k_B stands for Boltzmann's constant, and a_o is the distance an atom must jump over to attach/detach to/from the surface. The experimental data on diopside dissolution in diopside melt have been used by Alexander (2011) to show that the chemical reaction at the surface is an important step controlling dissolution. The model used estimations of the interface melt composition as well as the self-diffusion coefficients based on the ionic common-force (ICF) model of Liang et al. (1997). The discrepancy between the model predictions and the experimental data for andesite and picrite melts might originate in an inaccurate description of both the surface reaction and/or self-diffusion in the melts. This may arise from using experimental data which were controlled by both diffusion and convective transport. Additionally, Alexander (2011) suggested that the discrepancy might be related to (*i*) the errors of the MELTS software developed and optimized mostly for basaltic/mafic melts as well as (*ii*) to the errors affecting the diffusion coefficients and (*iii*) underestimates in the experimental temperatures. The discrepancy can be explained by the control of the slowest process between transport and the chemical reaction. This process is likely the diffusion of silica because it is the slowest-diffusing component in the aluminosilicate melt. Note that Equation 35 is similar to our principal equation relating dissolution rate to boundary layer melt viscosity. Our principal equation (Eq. 42, see below) was obtained based on isothermal experimental data on diffusion-controlled mineral dissolution.

4 Novel model based on experimental dissolution rates of the main rock-forming silicate minerals in aluminosilicate melts

4.1 Method of calculating mineral dissolution rates and the composition, viscosity, and mineral affinity of boundary-layer melts based on experimental data

To calculate the masses and volumes of the dissolved crystal and the composition of the boundary layer melt, we applied Equations 37 to 40. To calculate the corresponding viscosity of the boundary layer melt, we applied the MELTS 1.2.0 software at QFM redox conditions, where the melt viscosity is calculated according to the Shaw (1972) model. The melt viscosities lower than than 10^5 Pa s considered here are in excellent agreement (within 5 % uncertainty) with the recent experimental values of Giordano et al. (2008) (see Figures 3 and 5 of Giordano et al., 2008). The corresponding silica (SiO_2) and forsterite (Mg_2SiO_4) affinities of the boundary layer melts were estimated based on rhyolite-MELTS 1.0.2 (previous version allowing to estimate the affinities).

For the spherical (3D) runs, the following equations were applied:

$$m^{\text{Crystal}} = \rho\frac{4}{3}\pi\left[(r^\circ)^3 - (r^\circ - \Delta r)^3\right] \tag{37}$$

where m^{Crystal} (g) and ρ (g/cm^3) are the dissolved spherical crystal mass and density (the solid solution chemistry was suggested to be constant and corresponding to the starting composition), r° is the initial radius (cm) and Δr

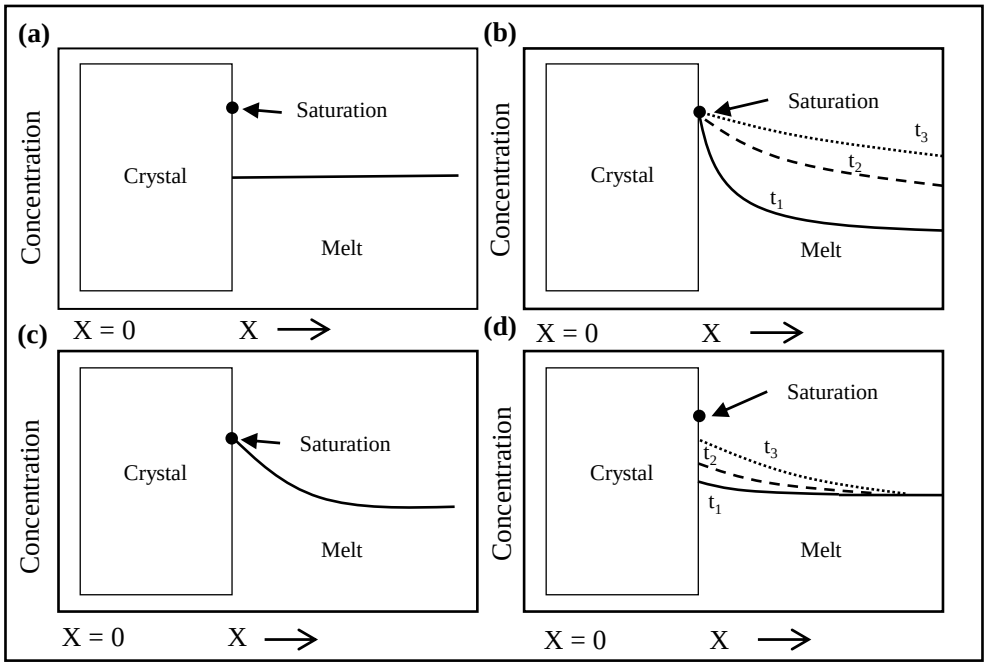

Figure 6. Evolution of the concentration of a crystal component as a function of the distance from the crystal surface during its dissolution in a melt: (a) crystal dissolution controlled by surface reaction in a well-mixed system; (b) crystal dissolution controlled by chemical diffusion, where the saturation composition is constant in infinite liquid, whereas it can be variable in the finite configuration; (c) transport-controlled dissolution (with formation of a diffuse layer) in a well-mixed system; (d) crystal dissolution controlled by surface reaction at the interface in an infinite non-mixed system (transport via diffusion). Modified from Zhang (2008).

is the sphere radius change during dissolution (cm) (Fig. 7). Alternatively, for the planar cylinder (1D) runs:

$$m^{\text{Crystal}} = \rho\pi r^{\circ 2}\Delta h \tag{38}$$

where Δh stands for the cylinder thickness change during dissolution (cm).

$$m_i^{\text{Crystal}} = 100 C_i^{\text{Crystal}} m^{\text{Crystal}} \tag{39}$$

where m_i^{Crystal} is the mass of the i^{th} oxide component in the dissolved crystal (g), C_i^{Crystal} is the concentration of the i^{th} oxide component in the crystal (wt%), and m^{Crystal} is the mass of the dissolved crystal (g) calculated from Equations 37 and 38.

$$C_i^{\text{Melt}} = 100\frac{m_i^{\text{Melt}} + m_i^{\text{Crystal}}}{m^{\text{Melt}} + m^{\text{Crystal}}} \tag{40}$$

where C_i^{Melt} stands for the concentration of the i^{th} oxide component in the boundary layer melt (wt%), m_i^{Melt} and m_i^{Crystal} are the bulk mass of the i^{th} oxide component (e.g., MgO) in the initial melt and dissolved crystal, respectively, and m^{Melt} and m^{Crystal} are the bulk mass of the initial melt and dissolved crystal, respectively. m^{Crystal} is calculated from Equation 38, whereas m_i^{Crystal} is calculated from Equation 39. The masses of the starting melt, where $m^{\text{Melt}} = \rho\pi r^{\circ 2}(h^{\text{Melt}} + \Delta h) \approx \rho\pi r^{\circ 2} h^{\text{Melt}}$ and $m^{\text{Melt}} = \rho\frac{4}{3}\pi((r^{\text{Melt}})^3 - (r(t))^3) \approx \rho\frac{4}{3}\pi(r^{\text{Melt}})^3$, are used for the calculations according to the available information on the initial configuration of the 1D (cylinder) or 3D (sphere) of the experimental charges, respectively. h^{Melt} and r^{Melt} are the initial glass length (for the cylinder) or radius (for the sphere), respectively, in the experimental configurations (Fig. 7). Alternatively, the mass of the initial melt was assumed based on the available information on the starting material configuration (e.g., $m^{\text{Melt}} = \rho\frac{4}{3}\pi(r^{\text{Melt}})^3 \approx 40$ mg) after Donaldson (1985, 1990). m_i^{Melt} was calculated as $m_i^{\text{Melt}} = \frac{C_0^{\text{Melt}} m^{\text{Melt}}}{100}$ during all calculations, where C_0 is the known concentration of the starting melt.

To calculate r, the mineral dissolution rate (mol cm^{-2} s^{-1}), based on the available experimental data, we used the equation:

$$r = \frac{V\rho}{M}/\{St\}\ (\text{mol cm}^{-2}\ \text{s}^{-1}) \tag{41}$$

where V (cm^3) and ρ (g/cm^3) are the volume and density of the dissolved mineral phase, respectively, M is the mineral molecular mass (g mol^{-1}), $S = \pi r_{\text{av}}^2$ (cm^2) refers to the dissolved mineral surface and the average radius ($r_{\text{av}} = (r^{\circ} + r(t))/2$) of the dissolved mineral sphere (3D), and t is the run duration. In the case of the fixed cylindrical crystal (1D), $S = \pi r^{\circ 2}$ (cm^2) (where r° is the cylinder radius for the mineral dissolution runs, Fig. 7).

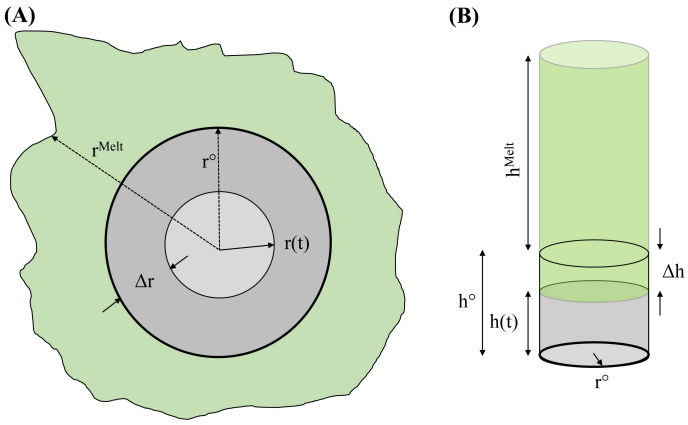

Figure 7. (a) Schema of spherical (3D) dissolution parameters, r° – initial radius, $r(t)$ – radius of the mineral sphere as a result of the dissolution reaction in time series experiments (t), and Δr – change in spherical radius due to the mineral dissolution. The initial melt (r^{Melt}) corresponds to the radius applied by using of wire loop experimental technique. (b) Schema of planar cylinder (1D) dissolution parameters, r° – initial (r° is considered to be constant) radius, $h(t)$ and h° – height of the mineral cylinder as a result of the dissolution reaction (t) and the initial height, respectively; and Δh –change in height of cylinder due to the mineral dissolution. The initial melt h^{Melt} represented by the green cylinder is applied by using of piston cylinder experimental technique.

4.2 New model based on experimental dissolution rates of the main rock-forming silicate minerals in aluminosilicate melts

In this section, we obtain dissolution rates from experimental run data available since 1985 for the main rock-forming silicate minerals in silicate melts. These experimental runs were used to extract dissolution rates which have been determined by measuring the size of the quenched time-series samples after the runs at high temperature and variable pressures (T, P). Edwards and Russell (1996) also reviewed these dissolution runs in their database, to which we have added experiments on congruent dissolution and models available since the late 1990s. In our review, we recalculated and used only primary data. The primary data considered here are: (1) temperature (T), (2) pressure (P), (3) run duration, (4) initial size and shape of starting mineral materials and the final size of the mineral allowing to calculate of the mineral dissolution rate (r), (5) the initial composition of the starting melt and the mineral allowing estimation of the initial properties of the melt (density and viscosity) and the reaction chemical affinity, (6) the uncertainty on the mineral dimension, and (7) experimental setups satisfying the approximation of a semi-infinite melt reservoir. For the sake of comparison, the results of dissolution experiments performed with minerals of spherical, cylindrical, and parallelepiped shapes were considered. To eliminate the difference in the mineral phase geometry, all appropriate dissolution rates are recalculated and expressed in units of mol cm^{-2} s^{-1}.

Unlike Edwards and Russell (1996), we did not apply linear regressions to the dissolution rate data to average the dissolution rate of a given mineral at given temperature-pressure conditions. Indeed, in most cases, mineral dissolution did not occur in an infinite melt reservoir (e.g., the far-field melt composition is different from the initial melt as illustrated in Fig. 3 and thus was likely controlled not only by diffusion but also by convection. We rejected data affected by convection-driven dissolution, which affects the long-duration runs, from our final consideration. Additionally, in the previous review of Edwards and Russell (1996), normalization was performed on data from experiments carried out with different crystal shapes. Edwards and Russell (1996) applied normalization of the dissolution rates to the molar volume and the number of oxygen atoms in the mineral formula to provide dissolution rates expressed in o.e.m. $cm^{-2}s^{-1}$ (oxygen equivalent moles). Finally, Edwards and Russell (1996) did not distinguish between diffusion- and convection-controlled experiments. Because of the strong dependence of the dissolution rate on temperature (degree of superheating, see below), the dataset considered here (Table S7) summarizes data on uniquely diffusion-controlled mineral dissolution in anhydrous and hydrous silicate melts of variable composition obtained at 1300 ± 20 °C and low pressures of < 1 GPa.

Figure 8 summarizes all recalculated dissolution rate data considered here obtained in time-series experiments of the same setup but of different duration (t, s). The quenched sample radius/dimension at each time was measured *ex-situ* to estimate dissolution rate, r [mol cm^{-2} s^{-1}]. These time-series experiments were performed principally with gas mixing autoclave/piston cylinder apparatuses (Tables S1–S10). Data of Thornber and Huebner (1985) for the dissolution of high-Mg olivine (Fo_{92} mol %) of rectangular shape are shown in Figure 8, but were not considered in the final equation (see below). Because of the relatively fast diffusion at high T–P, this experimental setup does not always satisfy the approximation of a semi-infinite melt reservoir, even at high initial melt-to-mineral ratio. The most complete datasets on the mineral dissolution rates include quartz and high-Mg olivine dissolution in rhyolite, andesite, basaltic and basanite melts. In addition, data for plagioclase, ortho- and clinopyroxenes, garnet are available (e.g., Donaldson, 1985, 1990; Thornber and Huebner, 1985; Brearley and Scarfe, 1986; Zhang et al., 1989; Donaldson, 1990; Shaw, 2000; Borisova et al., 2020b, Table 1, Tables S1–S10).

Table 1 summarizes all data considered in this work. For example, Donaldson (1985, 1990) used the spherical mineral dissolution (wire loop) method at 0.1 MPa in anhydrous melts of variable compositions (Fig. 8). In both datasets, dissolution rates were derived from measurements of the initial and final radii of the dissolving spheres with an uncertainty of ± 0.0035 cm on measurements. This is the most complete dataset available for Mg-rich-olivines ($Fo_{91.5}$ and $Fo_{88.5}$), quartz, and two types of plagioclase (An_{29} and $An_{52.5}$) in anhydrous basaltic, andesitic, and rhyolitic melts. To get reliable data at a constant temperature, in the present study we have selected only data obtained at

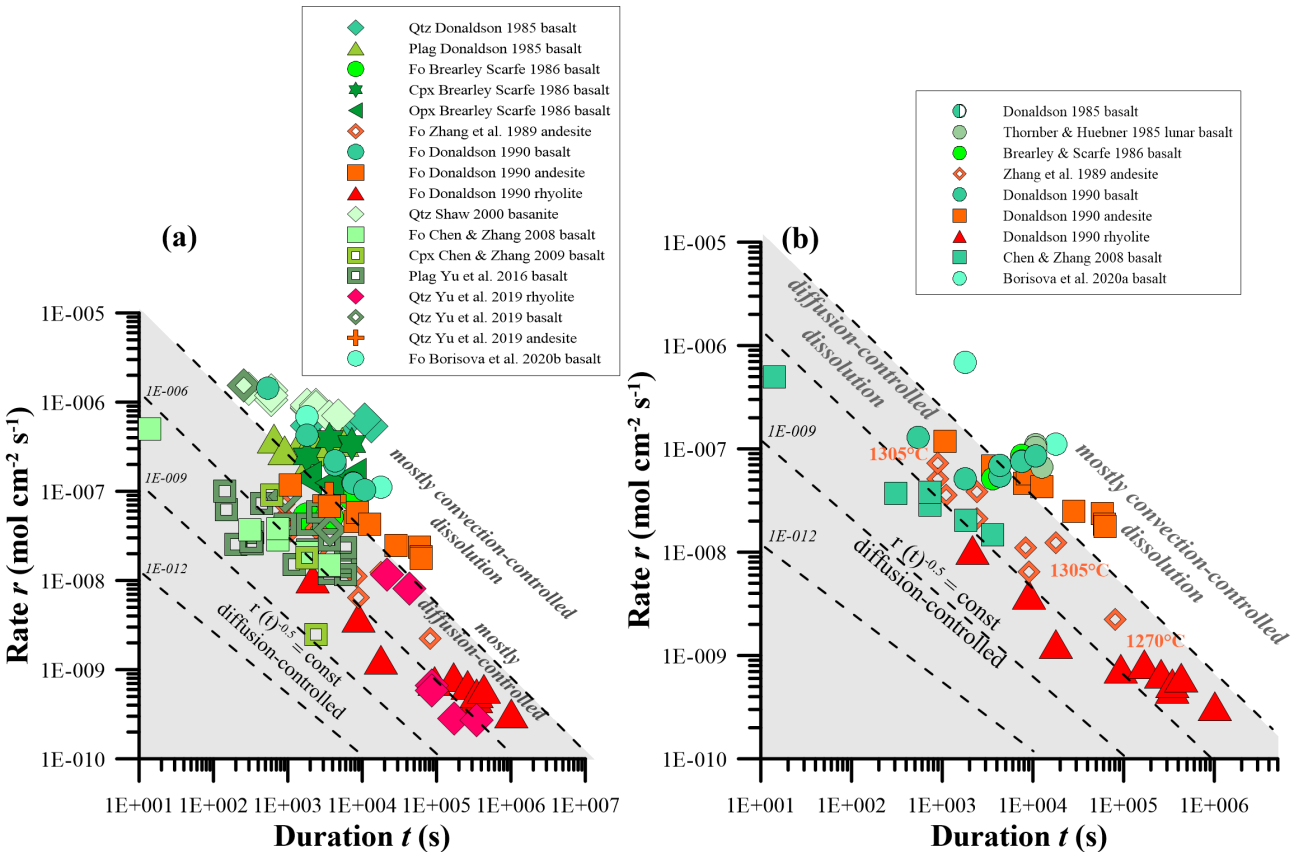

Figure 8. (a) Dissolution rate of the main rock-forming silicate minerals (Fo – forsteritic olivine, Qtz – quartz, Plag – plagioclase, Cpx – clinopyroxene, Opx – orthopyroxene) in aluminosilicate melts of variable compositions (basaltic, andesitic and rhyolitic) at constant temperature of 1300 ± 20 °C (< 1 GPa) as a function of the dissolution run duration (t, s). The data suggest that the silicate dissolution rates are near proportional to the reciprocal of the run duration, suggesting the diffusion-control transport mechanism. For example, 'Fo Donaldson 1990 basalt' refers to experimental work on forsterite dissolution in basaltic melt (Donaldson, 1990). All details are shown in Table 1, Tables S1–S10 (Borisova, 2026) for the calculation details. The grey areas correspond to the predominantly diffusion-controlled runs. The italic numbers correspond to the effective diffusion coefficients (D in $cm^2\,s^{-1}$) which should be corrected by the correction coefficient 3×10^{-9} (see the correlation coefficient in the correlation between dissolution rate in $mol\,cm^{-2}\,s^{-1}$ and $cm\,s^{-1}$, Table S10). Qtz – quartz, Plag – plagioclase, Cpx – clinopyroxene, Opx – orthopyroxene, Fo – high-Mg olivine. The colors of the symbols are chosen for their compositional sense: basaltic melt is green, andesitic melt is orange, and rhyolitic melt is red. (b) Dissolution rate (r, $mol\,cm^{-2}\,s^{-1}$) of high-Mg olivine (88–100 mol % Fo, forsterite-rich) in aluminosilicate melts of variable compositions (basaltic, andesitic and rhyolitic) at constant temperature of 1300 ± 20 °C as a function of the dissolution run duration (t, s). The time series parallel to the $r(t)^{-0.5}$ = const line are controlled by chemical diffusion, otherwise more complex mechanism controlled by both diffusion and convection happens. The grey areas correspond to the diffusion-controlled runs. The colors of the symbols are chosen for their compositional sense: basalt is green, andesite is orange, and rhyolite is red.

1300 ± 20 °C (Table 1). The silicate melts with lower initial SiO_2 contents (basaltic and andesitic) do not demonstrate significant variations in the viscosity of the boundary layer melts even if their MgO contents changed significantly with time, whereas forsterite dissolution is complicated by the convection effect for the longest runs of > 24 h.

Brearley and Scarfe (1986) performed dissolution of Mg-rich olivine, clino- and orthopyroxene, and garnet in alkaline basaltic melt over the ranges 1250–1500 °C and 0.5–3.0 GPa in a piston cylinder apparatus. Spherical crystals were used by these authors with an uncertainty of ±0.001 cm on radii measurements. Brearley and Scarfe (1986) also investigated the dissolution of olivine and pyroxenes. They concluded that olivine dissolution rate is equal to that of orthopyroxene at high pressure, whereas it is equal to that of clinopyroxene at low pressures. Here again, we use only data obtained at 1300 °C and pressures below 1 GPa.

Zhang et al. (1989) investigated the dissolution of cylindrical samples of San Carlos high-Mg olivine, synthetic forsterite, diopside, quartz, spinel and rutile in andesitic melts at 1215–1400 °C and 0.55–2.2 GPa in a piston cylinder apparatus. Only data obtained for silicate minerals (high-Mg olivines and quartz placed at the top, middle and bottom of the capsule) at 1270–1350 °C at 0.55 GPa were considered in the present work (Table 1).

Table 1. Summary on time-series experiments of silicate mineral dissolution in aluminosilicate melts.

Minerals	Number of experiments	Pressure	Authors	Composition of the initial melts*	Control on mineral dissolution
Olivine Mg_2SiO_4	120	0.1 MPa–2.2 GPa	Thornber and Huebner (1985) Donaldson (1985, 1990) Brearley and Scarfe (1986) Zhang et al. (1989) Chen and Zhang (2008)	Anhydrous basalt, andesite and rhyolite	Mostly diffusion
Olivine Mg_2SiO_4	2	0.5 GPa	Borisova et al. (2020b)	Hydrous basalt	Diffusion
Orthopyroxene $Mg_2Si_2O_6$	3	0.5–3.0 GPa	Brearley and Scarfe (1986)	Anhydrous basalt	Convection
Clinopyroxene $CaMg(Si_2O_6)$	3	0.5–3.0 GPa	Brearley and Scarfe (1986) Chen and Zhang (2009)	Anhydrous basalt	Convection except for short runs
Quartz SiO_2	70	0.1 MPa–2.2 GPa	Donaldson (1985) Zhang et al. (1989) Yu et al. (2019) Shaw (2000)	Anhydrous basalt, anhydrous andesite	Diffusion
Plagioclases Anorthite $CaAl_2Si_2O_8$	40	0.1 MPa–0.5 GPa	Donaldson (1985) Yu et al. (2016)	Anhydrous basalt	Convection and diffusion

* Complete dataset on the melt composition, experimental conditions and design is given in the Supporting Dataset Tables S1–S10 (Borisova, 2026).

Shaw (2000) studied the dissolution of quartz samples of different shapes in a basanite melt at 1350 °C and 0.5 GPa in different configurations (slabs at the top, bottom, and middle of the charge, and spheres) in high-pressure piston cylinder experiments. From this dataset, we selected, for coherency, only the results obtained for spherical quartz samples (Table 1).

More recently, the dissolution of cylindrical olivine, clinopyroxene, anorthite, and quartz in rhyolite, andesite and basaltic melts using piston-cylinder techniques mostly at 0.5 GPa but also up to 2.2 GPa pressure has been studied by Chen and Zhang (2008, 2009); Yu et al. (2016, 2019). From this dataset, we selected only results obtained at 1300 °C and ∼ 0.5 GPa for the time-series experiments.

Finally, Borisova et al. (2020b) performed serpentinite–basalt melt interaction experiments at 1300 °C and 0.5 GPa in a piston cylinder (Fig. 3). The cylinder of serpentinite and the basalt powder were placed in the upper and lower parts of the capsule, respectively. The results of this study showed dissolution of high-Mg olivine aggregate controlled by silica diffusion in the hydrous basaltic melt. The configuration of the experiment and the olivine-rich rock association of the dehydrated serpentinite allowed to describe forsterite dissolution in a water-bearing melt system (Table 1).

As illustrated in Figure 8, the rate of congruent dissolution of the main rock-forming silicate minerals for a given run decreases by about one order of magnitude as a function of the run duration. The data suggest that the main rock-forming silicate mineral dissolution rates are proportional to the reciprocal of the run duration, whereas diffusion-controlled time-series dissolution runs are in agreement with $r(t)^{-0.5} \approx$ const, where r is the dissolution rate and t is the dissolution run duration. Notably, the rates of mineral dissolution in basaltic and basanitic melts, represented by green colors, are higher than those of more felsic melts, such as andesitic and rhyolitic systems, represented by orange and red colors, respectively. Unlike felsic systems, which are only controlled by diffusion, numerous basaltic systems are controlled by both convection and diffusion.

Thus, to explore the effect of melt viscosity (below 10^5 Pa s), the boundary melt viscosity on the mineral dissolution rate is plotted in Figure 9. In this Figure, we have plotted as a function of the boundary layer melt viscosity (calculated in Section 4.1, Tables S1–S10) the average dissolution rates r (mol cm^{-2} s^{-1}) for the diffusion-controlled dissolution runs of high-Mg olivines, clinopyroxene, quartz and plagioclase, available for basaltic, andesitic to rhyolitic melts at 1300 ± 20 °C ($<$ 1.0 GPa) in the time-series experiments. The average dissolution rates of the silicate minerals at 1300±20 °C and $<$ 1 GPa pressures are found to be a function of the aluminosilicate melt viscosity according to:

$$r = k\eta^{-n} \quad (R^2 = 0.84) \tag{42}$$

where $k = 4 \times 10^{-7}$ (mol cm^{-2} s^{n-1} Pa^n) is the correlation coefficient, $n = 0.5$, and η (Pa s) is the boundary layer melt viscosity (lower than 10^5 Pa s). The longest ($>$ 24 h)

dissolution runs of forsterite in rhyolite melt from Donaldson (1990) were excluded from this plot because of anomalous dissolution complicated by convection effects. The data indicate that the viscosity of the boundary layer melts rarely increases in the time-series experiments on the same mineral and that the inverse correlation between the dissolution rate and run duration is not related to the increase in the boundary layer melt viscosity for most dissolution runs.

5 Discussion

5.1 Kinetic parameters controlling dissolution of the main rock-forming silicate minerals

Bunsen (1851) in the 1850s, joined by Daly (1925) in the early twentieth century and later by Bowen (1928), were the first to introduce terms related to open-system processes in the description of magmatic processes (partial melting, mineral dissolution, magma mixing, crustal assimilation). For more information on basic terms and parameters involved in the mineral dissolution process, see Section 2.1. Experimental measurements may be divided into three groups.

(1) Diffusion-controlled dissolution, as assessed by a variety of tests: (i) A change in sample thickness (or dissolution distance) that is proportional to the square root of run duration (Kuo and Kirkpatrick, 1985b; Zhang et al., 1989; Donaldson, 1990; Liang, 1999; Acosta-Vigil et al., 2006a,b). In this case, the dissolution is controlled by the rate of diffusion in the aluminosilicate liquid across a boundary layer that forms at the crystal–melt interface. (ii) The function $\mathrm{erf}^{-1}(1 - C_x/C_o)$ is a linear function of distance (where C_x is a given concentration in an elemental profile and C_o is the interface melt concentration of a given element; e.g., Harrison and Watson, 1983; Yu et al., 2016; Borisova et al., 2020a). (iii) Concentration gradients in a given experimental sample (from profiles or elemental maps) are monotonic and show no signs of convection; (iv) diffusion coefficients are independent of time; (v) the dissolution rate (r) multiplied by the square root of run time is constant (Fig. 8). For example, high-Mg olivine dissolution rates of Zhang et al. (1989) at 1300 ± 50 °C (at variable temperatures of 1270, 1285, 1305, 1315 and 1350 °C) follow the same trend of dissolution rate as a function of time as the high-Mg olivine dissolution rates measured in experiments using most designs and techniques (e.g., wire loop-based and piston cylinder-based methods). This may indicate that such factors as temperature were controlling diffusion-controlled dissolution during the experiments of Zhang et al. (1989). The authors also quantified the extent of the crystal–melt interface reaction through numerical solutions of the diffusion equation. For this purpose, they developed a reaction-diffusion equation which treats both the interface reaction and diffusion in the melt. Based on this analysis, much later, Zhang's group demonstrated that in most of his group's runs crystal dissolution was diffusion-controlled. The authors showed that diffusive dissolution can be mathematically solved and they estimated diffusive dissolution rates using the EBDC of principal components (e.g., Liang et al., 1996). Technically, diffusion coefficients can be extracted from the concentration profiles of quenched glasses produced during mineral dissolution experiments and measured analytically (e.g., by electron probe microanalysis, taking into account secondary fluorescence effects produced by electron probe microanalysis, Borisova et al., 2018, 2020a). Consideration of these analytical methods is beyond the scope of this paper.

(2) In case of surface reaction control, the change in crystal radius/thickness is proportional to time, and the dissolution rate is independent of time. An example of this control is provided by quartz sphere dissolution in basaltic melt (Donaldson, 1985). In fact, surface reaction control on the mineral dissolution rate is observed for mineral phases with compositions similar to the melts (e.g., Kerr, 1995), because the chemical affinity approaches zero in this case uniquely at temperatures close to the melting point. However, no study has been performed far from equilibrium to check if the surface reaction is always slow enough (slower than diffusion) to control mineral dissolution. For example, diopside dissolution in diopside melt is controlled by the surface reaction (Kuo and Kirkpatrick, 1985a). Surface reaction control is also observed in low melt-to-rock ratio systems during partial melting and the following dissolution of two SiO_2-rich minerals with very different dissolution rate constants such as quartz and phlogopite (Hammouda and Pichavant, 1999). These authors predicted that the melt heterogeneity diminishes and dissipates when one of the mineral reactants is consumed. Thus, the surface reaction may be predominant close to equilibrium when the chemical affinity of the reaction is small enough to make the chemical reaction flux smaller than the diffusion flux. Importantly, Acosta-Vigil et al. (2002) and Shaw (2000, 2004, 2006) indicated that interface reaction is the rate-controlling factor for the dissolution of Al- and Si-rich minerals such as corundum, andalusite and quartz in aluminosilicate melts. This may be explained by the fact that increasing SiO_2 content (increasing the melt viscosity) in the boundary-layer melts could decrease the surface reaction rate (see Donaldson, 1990). Once the dissolution rate drops below a critical value, diffusion becomes faster than the surface kinetics and diffusion no longer controls mineral dissolution (Shaw, 2000).

However, the surface reaction control of silicate mineral dissolution in these felsic systems is in contradiction with the data of Cooper Jr and Kingery (1964) and Liang (1999) showing the rapid attainment of diffusional control in the course of sapphire and quartz (and quartzite) dissolution in silicate melts of the $CaO-Al_2O_3-SiO_2$ (CAS) system. Liang (1999) claimed that chemical equilibrium at the crystal–melt interface was rapidly attained for the timescale of $t > 0.3$ h at 1500 °C. The control of dissolution in those Si-Al-Ca-rich systems by surface reaction likely depends on the saturation state of the melt with respect to the mineral phases. When an interface reaction controls mineral dissolution, the rate depends on the reaction mechanism and the crystal may display anisotropic dissolution behavior

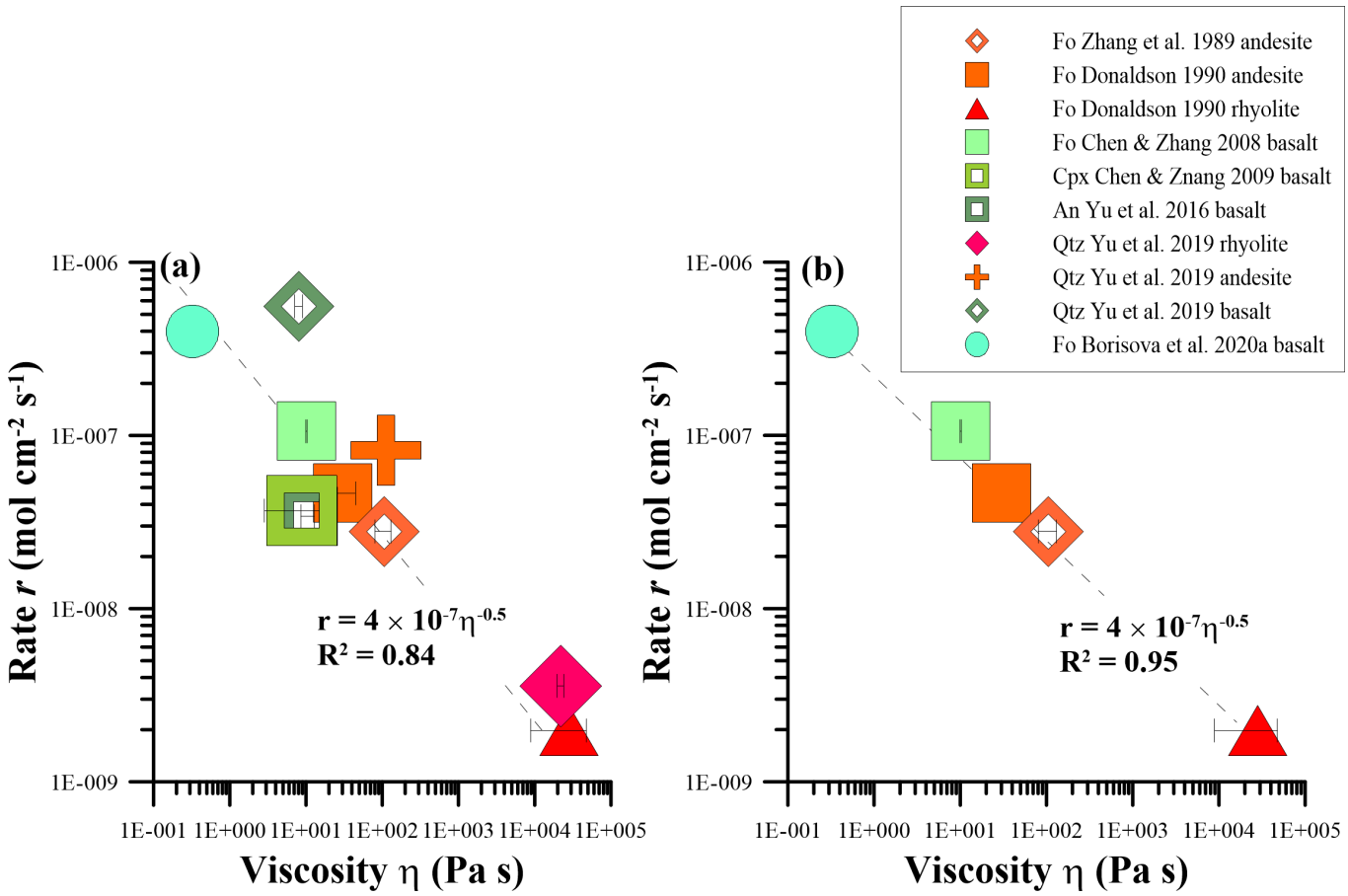

Figure 9. (a) Average rates of diffusion-controlled dissolution of spherical (3D) and cylindrical (1D) samples of the main rock-forming silicate minerals (olivine, quartz, pyroxenes and anorthite), r (mol cm^{-2} s^{-1}), in basaltic, andesitic to rhyolitic melts at 1300 ± 20 °C and low pressures (< 1.0 GPa) versus boundary layer melt viscosity calculated based on the MELTS software. For example, high-Mg olivine (88–94 mol % Fo) or forsterite (Fo) dissolution runs of 'Fo Donaldson 1990 andesite' refer to experimental work on forsterite dissolution in andesitic (andesite) melts (Donaldson, 1990). An – anorthite, Qtz – quartz, Plag – plagioclase, Cpx – clinopyroxene, Fo – high-Mg olivine. The colors of the symbols are chosen for their compositional sense: basaltic melt is green, andesitic melt is orange, and rhyolitic melt is red. (b) Average rates of diffusion-controlled dissolution of spherical and cylindrical Mg-rich olivine (Fo), r (mol cm^{-2} s^{-1}), in basaltic, andesitic to rhyolitic melts at 1300 ± 20 °C and low pressures (< 1.0 GPa) versus final melt viscosity calculated based on the MELTS software (Tables S1–S10). The colors of the symbols are chosen for their compositional sense: basalt is green, andesite is orange, and rhyolite is red.

(Zhang, 2013). In contrast, when mass transfer controls the dissolution reaction, the reaction is isotropic.

(3) Convection controlled dissolution involving mass transfer leads to constant dissolution rates and the development of steady-state concentration profiles in the diffuse layer at far from equilibrium conditions (e.g., Zhang et al., 1989; Zhang, 2008). In early experimental studies of Scarfe et al. (1980) and Brearley and Scarfe (1986), convection has likely affected mineral dissolution, resulting in inaccurate values for chemical diffusivities derived from these experiments as pointed out by Chen and Zhang (2009). Convection accelerates dissolution rate because it decreases the thickness of the diffuse layer present at the solid–melt interface. The convection-driven experiments, such as several long duration runs, are not considered nor explored in this review.

5.2 Role of melt affinity

For aluminosilicate melts, A, the chemical affinity reported in J mol^{-1} for a given mineral saturation in a melt was calculated at given physical-chemical conditions (P–T–f_{O_2}–a_{H_2O}) using the rhyolite-MELTS thermodynamic code (Section 4.1) and the composition of the boundary layer melt in which the mineral is dissolved. For a given mineral phase, A is a function of the melt composition, which may in turn be related to the melt structure, typically expressed for silicate melts by the ratio NBO/T (nonbridging oxygens per tetrahedrally-coordinated cations) (e.g., Shaw, 2006, 2012 and references therein). These affinities were then plotted as a function of dissolution rate (Fig. 10). This Figure demonstrates that while the deviation from equilibrium could be argued to be the driving force for mineral dissolution when considering a single set of experiments, when all data are considered together the situation is far less clear. For

example, the apparent dissolution rates for the time-series experiments of Donaldson (1985, 1990) and Thornber and Huebner (1985) are approximately constant and approach 10^{-7} mol cm^{-2} s^{-1} for a range of calculated chemical affinity. Furthermore, strongly decreasing dissolution rates at a constant chemical affinity are observed by Zhang et al. (1989) and Chen and Zhang (2008) for olivine dissolution. This is likely due to the temperature effect rather than a significant impact of chemical affinity, which remains nearly constant for similar boundary layer melt compositions (Table S7). Overall, there is no clear correlation between affinity and dissolution rate (Fig. 10). However, when close to equilibrium, the dissolution rates of silicate minerals in the melts are driven by chemical affinity. In this case, dissolution is controlled by surface reactions rather than diffusion.

5.3 Effect of melt viscosity on silicate mineral dissolution rates in planetary and geological melts

Figure 9 demonstrates that the experimental dissolution rate may be described as a simple function of the viscosity of the boundary layer melts: the higher the viscosity, the slower the dissolution rate. Figure 9b shows the same relation for high-Mg olivine dissolution. While a secondary role of additional factors (such as chemical affinity) cannot be excluded, viscosity clearly plays a central role. A similar conclusion has recently been reached based on consideration of alumina (Al_2O_3) dissolution in silicate melts by Yoshizawa et al. (2025). The observed correlation between dissolution rate and the boundary layer melt viscosity demonstrates that low-viscosity magmas are far more prone to contamination by lithosphere materials than high-viscosity felsic magmas. Indeed, an addition of alkaline elements (e.g., K, Na) to the silicate melt leads to a significant change in the mineral dissolution rate if this addition affects the melt structure in terms of the non-bridging oxygen to tetrahedral cations (NBO/T) ratio (Shaw, 2006). This author proposed that the silica activity in the melt defines the maximal value of the dissolution rate, whereas the melt viscosity determines whether this maximum value may be achieved in the case of diffusion control (Shaw, 2006). The viscosity control described by Figure 9 is in perfect agreement with the conclusion of Shaw (2004), inferring that dissolution rates should decrease with increasing silica activity and viscosity. The lower viscosity of carbonatitic or basaltic melts at deeper mantle levels also explains the high reactivity of these melts (Kono et al., 2014), which have a higher dissolution rate for the silicate minerals and are therefore able to assimilate large masses of lithosphere rock material, although other mechanisms such as surface reaction control can have an important role at high pressures and temperatures.

Silicate mineral dissolution rates follow an inverse square root function of the viscosity in the boundary layer melt (Fig. 9). This inverse dependence is not controlled by the nature of the dissolving mineral and is observed for different silicates such as forsterite, plagioclases, pyroxenes and quartz. The inverse correlation signifies that the rate of dissolution is a direct function of the dynamic transport properties of the boundary layer melt. In the runs with high-Mg olivine, the dissolution rate is either constant or decreases with the run duration in each experimental setup (Fig. 8), suggesting that changes in the composition of the boundary layer melt (in comparison to the composition of the initial melt) occur during the run. Such a relationship between the mineral dissolution rate, the melt viscosity and the run duration suggests that, irrespective of how far the system is from thermodynamic equilibrium, the melt viscosity (which controls transport properties such as diffusion) is the main controlling factor of the mineral dissolution rate.

Viscosity is a physicochemical parameter directly related to the diffusivity of network-forming elements such as Si and O (Mungall, 2002). This relation is expressed by the Eyring equation (Eq. 20). Therefore, Equation 20 allows for a first-order prediction of the dissolution rates and can be expressed as:

$$r = k\frac{1}{\sqrt{\eta}} = k\frac{\sqrt{D_i\lambda}}{\sqrt{k_B T}} \approx k'\sqrt{D_i} \qquad (43)$$

where r stands for the mineral dissolution rate (mol cm^{-2} s^{-1}), $k = 4 \times 10^{-7}$ mol cm^{-2} s$^{-0.5}$ Pa$^{0.5}$ is the correlation coefficient, η is the viscosity (Pa s), D_i is the diffusion coefficient of the network-forming elements (cm^2 s^{-1}), $T = 1573.15$ K is constant, and $k' = \frac{k\sqrt{\lambda}}{\sqrt{k_B T}}$ is a constant (mol cm^{-3} s$^{-0.5}$) related to the Boltzmann constant k_B (m^2 kg s^{-2} K^{-1}), and λ is the characteristic particle translation distance (Å). Geological and planetary melts may be more complex multicomponent systems than those modeled by the Eyring relation, which well describes the diffusion of the main network-formers in silicate melts (Dingwell and Webb, 1990). Thus, silica and oxygen diffusion and Si−O breakdown in aluminosilicate melts are the main factors controlling the dissolution of silicate minerals. The higher the melt viscosity and the slower the Si−O breakdown in aluminosilicate melts, the slower the dissolution rate of the silicate minerals according to Equations 42 and 43 (Fig. 9).

Morgan and Liang (2003) have proposed diffusive control (Si diffusion) on the harzburgite dissolution rate. The effective binary diffusion coefficient (EBDC) constrained experimentally by Guo and Zhang (2016) at 1500 °C and 1 GPa also indicates that the slowest diffusing component (eigenvector, see Section 2.2.4) is due to the exchange between Si and Al, suggesting that silica (and aluminum) diffusional transport is the main rate-controlling mechanism during the dissolution of silicate minerals in silicate melts (e.g., Guo and Zhang, 2020). Recently, Borisova et al. (2020b) demonstrated that the dissolution of a high-Mg olivine aggregate in hydrated basaltic melt was mostly controlled by silica diffusion in the melt. Thus, the extant literature indicates that the diffusion of network-forming ions, including but not limited to Si, O, and occasionally Al, should be the primary factor regulating the rate of dissolution of the predominant silicate minerals within the lithosphere.

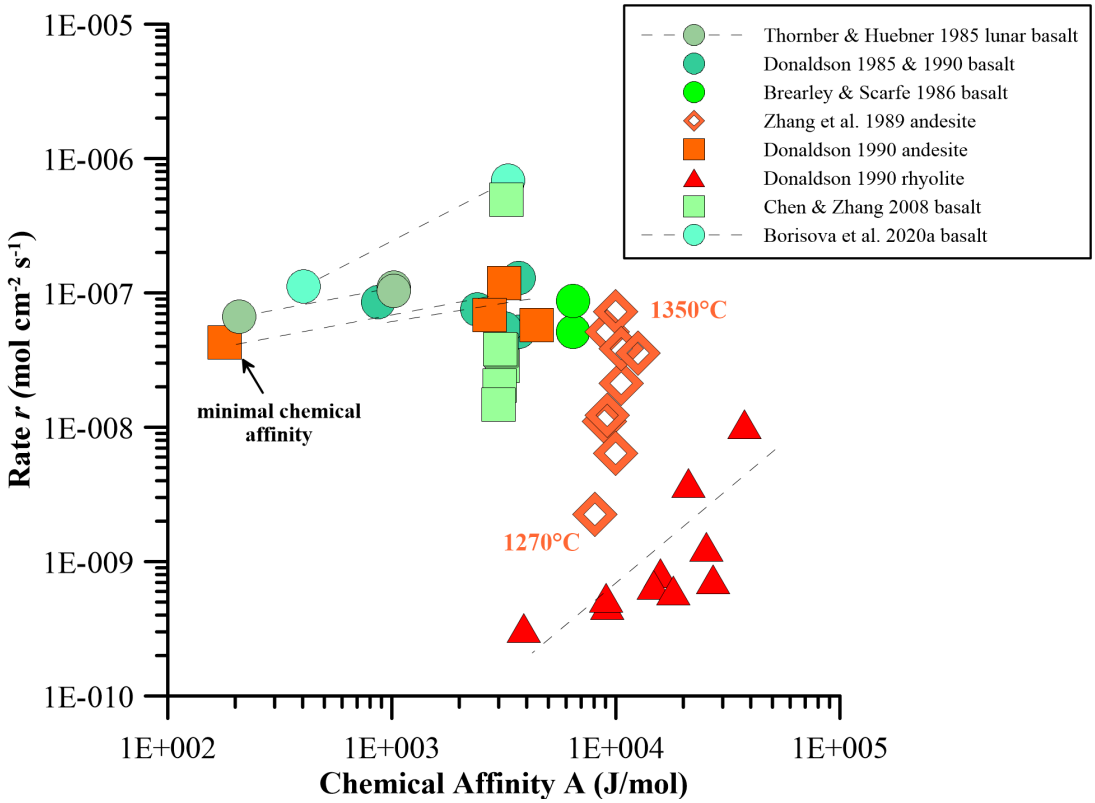

Figure 10. Diffusion-controlled dissolution rates for Mg-rich olivine, r (mol cm^{-2} s^{-1}), in silicate melts at 1300 ± 50 °C versus chemical affinity, A (J mol^{-1}), of the boundary layer melts calculated based on the MELTS software (Tables S1–S10). For example, 'Fo Borisova et al., 2020 basalt' means the data on the boundary layer melts produced during time-series runs on high-Mg olivine dissolution in tholeiitic basaltic melt (Borisova et al., 2020b). High-Mg olivine (88–94 mol % Fo) refers to experimental work on forsterite dissolution in andesitic (andesite) and rhyolitic (rhyolite) melts (Donaldson, 1990). The calculated chemical affinities (A) data are given in Tables S1–S10. The colors of the symbols are chosen for their compositional sense: basalt is green, andesite is orange, and rhyolite is red.

5.4 Redox and temperature control

Redox conditions likely control the planetary melt structure and the melt viscosity either due to oxygen incorporation in the melt as an incompatible element or due to a change in the $Fe^{3+}/\Sigma Fe$ ratio affecting the silicate melt structure and degree of the melt polymerization (Dingwell and Virgo, 1987; Lin et al., 2021, 2022; Casas et al., 2023). It was demonstrated by Dingwell and Virgo (1987) that the redox conditions considerably change the melt structure with respect to Fe (network former or network modifier) and that melt viscosity strongly depends on the degree of the melt polymerization, NBO/T. Thus, redox effects should influence the silicate mineral dissolution rate. In addition, as the temperature and degree of superheating (temperature above the liquidus) increase, the rate of mineral dissolution increases. This can be a direct effect of the decreasing viscosity of the melt (Di Genova et al., 2023) and thus the increasing chemical diffusivities at higher temperatures. In this context, mineral dissolution is a critical reaction in magmatic processes at conditions where liquidus minerals (minerals existing in equilibrium with silicate melt on a melt liquidus) are subjected to superheating (superheating being the temperature difference between a given temperature and the melt liquidus; Kuo and Kirkpatrick, 1985a). Superheating occurs during the majority of magmatic processes such as magma mixing and hybridization, anatexis, and incorporation of xenoliths into the magma, as well as during decompression. Kuo and Kirkpatrick (1985a) have shown that it exerts an important control on crystal dissolution due to changes in the melt structure with increasing temperature and pressure (i.e., Mysen et al., 1979). Kuo and Kirkpatrick (1985a) demonstrated that the main silicate mineral dissolution occurs most extensively at shallow lithospheric depths (< 50 km), suggesting strong compositional control of the ultramafic mantle material on the percolating basaltic melt composition. This conclusion aligns with the primary equation (Eq. 42) derived in this study.

6 Implications for mantle-derived magma-lithosphere interactions

6.1 The lithosphere assimilation by mantle plume-derived melts

In most experimentally based models of mineral dissolution (Liang, 1999, 2000, 2003) and basaltic melt–peridotite interaction experiments, it has been established that the mineral dissolution rates are controlled by the rate of diffusion of the main network-forming components (silica,

oxygen) in melts (e.g., Morgan and Liang, 2003, 2005; Morgan et al., 2006; Borisova et al., 2020b, 2021a). This is in agreement with Equation 43. However, very few studies have investigated high-temperature mineral dissolution mechanisms at the nanometric to atomic scales (e.g., Konrad-Schmolke et al., 2018). Konrad-Schmolke et al. (2018) proposed that hydration reactions during eclogite-stage natural transformation involved the depolymerization of the crystal lattice and repolymerization of the amorphous material at the mineral surface, allowing for the control of element transport and mineral reaction rates. However, this mechanism involving aqueous fluids cannot be applied to mineral dissolution in silicate melts. Based on the well-known behavior of aluminosilicate melts with decreasing viscosity at high pressures (Wolf and McMillan, 1995) and on Equation 42, we can conclude that the lithosphere-forming silicate minerals will be much more easily dissolved in low-viscosity magmas at high pressures. Additionally, a mineral-bearing rock would dissolve faster in a dynamic convection-driven system compared to a static and diffusion-driven system.

Another aspect of silicate mineral dissolution in geological and planetary melts is the melt-to-rock ratio during melt percolation through the rock. This parameter could also be rate-controlling if the system follows reactive porous flow with low melt-to-rock ratios (e.g., Cambeses et al., 2023) or melt channelization with high melt-to-rock ratios (Morgan and Liang, 2005; Pec et al., 2015, 2017, 2020). The rate of mineral dissolution thus can depend on the melt-to-rock ratio in natural systems and the style of melt percolation in planetary rocks. In a simplified model where the deepest parental melts have low viscosity (e.g., Wolf and McMillan, 1995; Kono et al., 2014, see references therein), deep mantle plume melt percolation to the surface through channelization can be considered. The application of Equation 42 enables the estimation of the volume of assimilated rocks during isothermal assimilation by mid-ocean ridge basalt (MORB) or ocean island basalt (OIB).

Figure 11 illustrates the lithospheric assimilation of OIB melts with a viscosity ranging from 0.01 to 10 Pa s. With a mineral dissolution rate ranging from 6×10^{-8} to 2×10^{-6} mol cm^{-2} s^{-1} (according to Eq. 42) and a surface area of 1 km^2, up to 0.05 km^3 of silicate mineral material would be assimilated in one year. Therefore, the volume of crustal or mantle rock assimilated by the parental melts of OIB may be significant: the lower the viscosity, the higher the degree of lithosphere assimilation. In addition to mantle plume-derived OIB, percolating MORB melts are low-viscosity melts with an elevated proportion of the carbonate component (Kono et al., 2014; Borisova and Tilhac, 2021 and references therein). Numerous evidences for melt–rock reactions are described in the ophiolite mantle–crust transition zone and the mid-ocean ridge setting represented by depleted basalts, dunites and chromitites produced in spreading settings (Borisova et al., 2012; Zagrtdenov et al., 2018; Rospabé et al., 2019; Borisova et al., 2020b), as well as in mantle plume-derived OIB (Borisova et al., 2017, 2023 and references therein). Thus, the geochemical and isotopic effect of the lithosphere assimilation of parental mantle-derived melts through the mantle-derived melt percolation is an important issue when interpreting the composition of MORB and OIB in terms of the mantle source composition.

6.2 Perspectives and implications for the minerals dissolution at depth

A kinetic investigation of planetary melt–rock interactions is necessary to better understand diffusion- and convection-controlled reactions, as well as surface reactions and rate-controlling mechanisms of deep systems with variable melt-to-rock ratios under a wide range of pressures. This is necessary to generate new predictive kinetic models in association with available thermodynamic models. New analytical methods, such as atom probe tomography and transmission electron spectroscopy, in conjunction with first-principles dynamic molecular modeling, will enable us to understand the mechanisms of interface reactions, chemical and isotopic exchanges, and elemental and isotopic partitioning. This will allow us to study the kinetics of melt–fluid–rock and magma–rock interactions, which control processes such as partial melting, magma hybridization, lithospheric assimilation, and mantle metasomatism.

For example, most minerals of metamorphic rocks are not in thermodynamic equilibrium with silicate melt at magmatic conditions. As a result, the reactions of partial melting and dissolution are irreversible, although the transition stage mineral phases and their associations may approach thermodynamic equilibrium with the silicate melt at magmatic conditions. Borisova et al. (2020b, 2021a) and Basch et al. (2025) demonstrated that the assimilation rate and reaction mechanisms are also dependent on the melt migration style and melt-to-rock ratio in a given system. The first step is the dehydration/decomposition of the metamorphic minerals and their associations and the formation of fluid-rich silicate and/or carbonate phases (e.g., Borisova and Bohrson, 2023). For example, the mechanisms of metapelite melting reactions are strongly controlled by water activity (Brearley, 1987; Rubie and Brearley, 1987; Johannes, 1989). The available experimental data allow predicting that the dissolution of hydrated mantle (e.g., serpentinite) rocks in geological melts is a relatively rapid process controlled by silica diffusion (Borisova et al., 2020b, 2021a,b).

A preliminary series of high-pressure experimental studies on peridotite dissolution in eclogite-derived melts, as well as the reaction of pyroxenite with peridotite to form mafic cumulates, has become available (Wang et al., 2020; Borghini et al., 2022; Klaver et al., 2024). These studies examined reactions of pyroxenite with mafic pressures ranging from 1 to 2 GPa and higher. These studies have implications for terrestrial subduction processes, carbonated mantle magmatism, and extraterrestrial mantle processes. However, only preliminary information exists on the kinetic parameters (e.g., rates, mechanisms, and timescales) of reactions involving metamorphic crustal rocks (e.g., carbonated basalt; Thomson et al., 2016) and mantle peridotite rocks in the deep mantle. A significant advancement in

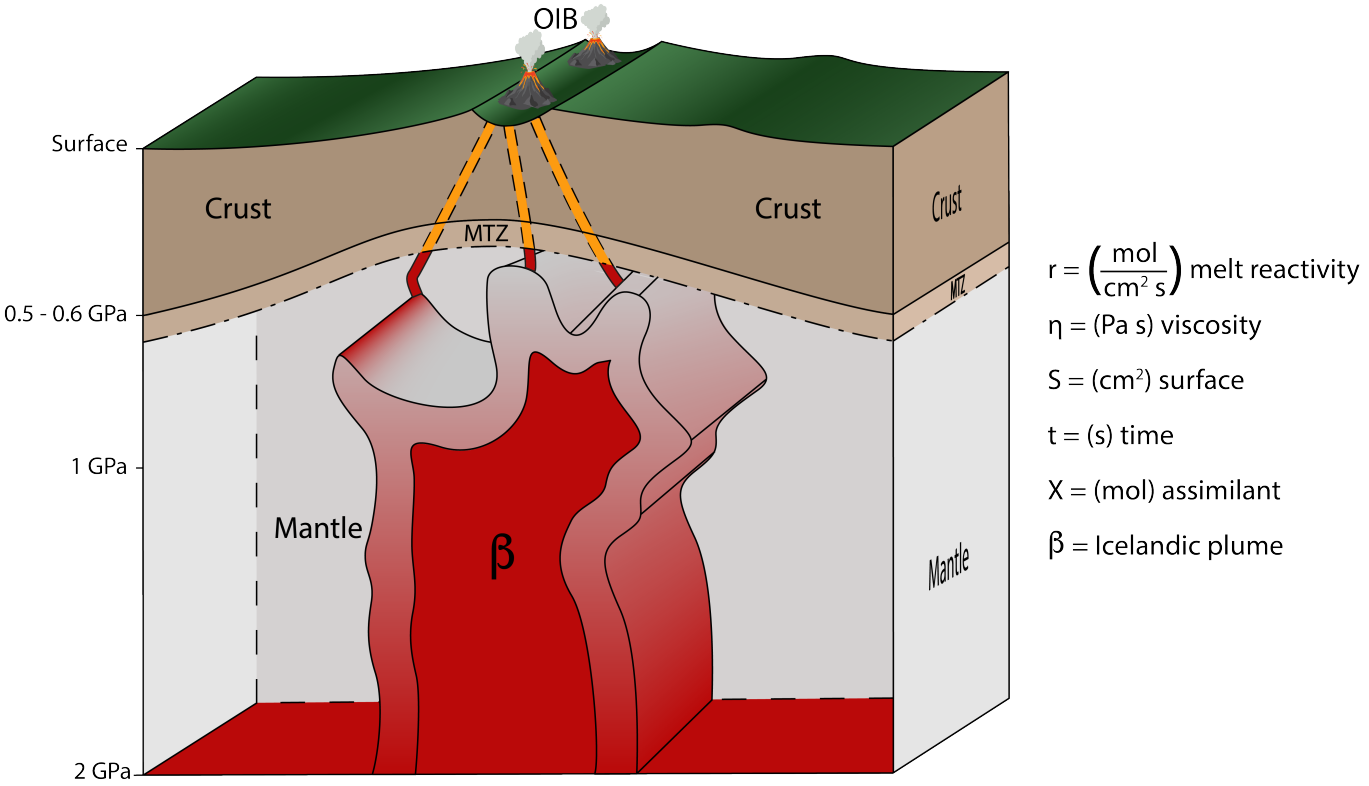

Figure 11. Schema of the Icelandic plume-lithosphere interaction model illustrating assimilation of deep percolating partially melted plume material of basaltic composition (β, Icelandic plume) and representing the ocean island basaltic melt reaction with lithosphere material. Equation 42 for the main silicate dissolution and the corresponding parameters (r, η, S, t) are applied to estimate the maximal quantity of the assimilated material in moles (X) and the corresponding mass of the lithosphere assimilated upon the percolating melt reaction with the lithosphere. MTZ is the mantle–crust transition zone (e.g., Borisova et al., 2017, 2020b, 2021b).

the field will be the development of kinetic models and the experimental characterization of the kinetic parameters that govern mineral–melt reactions in the mantle of Earth and other planets.

7 Conclusions

1) Available experiments on silicate mineral dissolution in aluminosilicate melts applicable to planetary lithosphere assimilation by magmas, magma mixing, as well as the modeling of mantle metasomatism and other processes of melt–rock and magma–rock interactions have been reviewed. Most kinetic experiments on aluminosilicate mineral dissolution in silicate melts are consistent with the semi-infinite reservoir condition, although experimental limitations often cause major difficulties in interpreting the results. To experimentally model porous flow, the melt-to-mineral ratio should be small, whereas to model melt channelization, the initial melt-to-mineral ratio should be as high as possible, the run duration as short as possible and optimal for a given experimental charge. The application of piston cylinder experiments at elevated pressures is preferable to that of the wire loop technique at atmospheric pressure because of the more stable configuration of the dissolving assemblage and a resulting diffusional or convective control of mineral dissolution, although convective mechanisms may dominate at pressures higher than 1 GPa.

2) Mineral and rock dissolution in geological and planetary melts is controlled by diffusional transport rather than chemical reaction at the crystal surface, at least at pressures below 1 GPa. Diffusion of network-forming ions such as silica, oxygen and aluminum in the melts is the rate-controlling factor during the diffusion-controlled dissolution of silicate minerals in experiments at elevated pressures. The diffusion-controlled dissolution rate, r (mol cm^{-2} s^{-1}), of spherical and cylindrical anhydrous silicate mineral samples (forsterite, diopside, plagioclases, and quartz) is found to be a function of the viscosity of the boundary layer melts, with no dependence on the nature of the dissolving silicate mineral. The diffusion-controlled dissolution rate (r) of silicate minerals (e.g., olivine, pyroxenes, plagioclase and quartz), irrespective of how far the system is from thermodynamic equilibrium, can be described by the following equation at 1300 ± 20 °C and < 1 GPa conditions:

$$r = k\eta^{-0.5} = k\frac{1}{\sqrt{\eta}} \approx k'\sqrt{D} \qquad (44)$$

where the correlation coefficient $k = 4 \times 10^{-7}$ (mol cm^{-2} s^{n-1} Pa^{n}), η (Pa s) is the boundary layer melt viscosity, and $k' = \frac{k\sqrt{\lambda}}{\sqrt{k_B T}}$ is a constant (mol cm^{-3} s$^{-0.5}$) related to the Boltzmann constant k_B (m^2 kg s^{-2} K^{-1}), $T = 1573.15$ K is

the temperature, λ is the characteristic particle translation distance (Å) and *D* is the diffusion coefficient of the network formers Si and/or O (and eventually Al or Zr as network formers). This relation shows that low-viscosity mafic–ultramafic magmas can be significantly more contaminated by lithosphere rock material compared to high-viscosity felsic magmas. This correlation for the main rock-forming minerals may be directly applicable to planetary lithosphere assimilation by magmas, magma mixing, as well as the modeling of mantle metasomatism or other types of melt–rock interactions (Zagrtdenov et al., 2015).

3) The low viscosity of geological and planetary melts at deep mantle levels implies that large masses of the mantle material may be assimilated by melt during percolation to the surface. At higher pressures and temperatures, the decreasing melt viscosity and increasing diffusivity of network former elements (Si, O) should increase the rate of mineral dissolution through mantle assimilation by upwelling melts and the dissolution rate is slowing down at the planetary surface due to increasing viscosity of the shallower melts. Since the deepest parental melts of the mid-ocean ridge basalts (MORB) and ocean island basalt (OIB) are low-viscosity melts, an important geochemical problem of the MORB and OIB composition interpretation is a strong effect of lithosphere assimilation by the melts *via* the melt percolation in the lithosphere. An expanded database for the main rock-forming silicate minerals at higher pressure conditions (> 1 GPa) is necessary to describe mantle assimilation by planetary magmas, melt mixing as well as modeling of genesis of diverse types of mantle-derived magmas.

4) In the near future, the kinetic investigation of planetary melt–rock reactions should focus on improving our understanding of diffusion-, convection-, and surface-controlled reactions, as well as the rate-controlling mechanisms of deep systems with variable melt-to-rock ratios under a wide range of pressures (Borisova et al., 2025). Additionally, new predictive kinetic, geochemical, and isotopic models should be generated in conjunction with available thermodynamic models. New kinetic experiments and analytical methods such as atom probe tomography in association with the first principles dynamic molecular modeling will allow understanding the mechanisms of the interface reactions, chemical and isotopic exchanges such as partitioning. In summary, investigating the kinetics of melt-fluid-rock and magma-rock interactions is necessary to understand partial melting, magma hybridization, lithospheric assimilation, and mantle metasomatism on Earth and other planets.

Acknowledgments

This research was supported by Institut national des sciences de l'Univers - Centre National d'Études Spatiales PLAGIOGRAN grant (INSU-CNES, France; 2022–2023), Felsic_Planeta grant (Observatoire Midi-Pyrenees, 2024) to A.Y.B. This article is funded by the European Union (ERC, PLANETAFELSIC, project 101141259) to AYB (2025–2030). Views and opinions expressed are however those of the author(s) only and do not necessarily reflect those of the European Union or the European Research Council. Neither the European Union nor the granting authority can be held responsible for them. The authors thank S. Lambart, P. Asimow and J. Dixon, C. M.O'D. Alexander, B. Edwards, J. Fehrenbach, Y. Liang, M. Ghiorso, I. N. Bindeman, B. Scaillet, C. Martel, and Y. Zhang as well as numerous anonymous reviewers for important suggestions and comments on the initial versions of this manuscript.

Data, code, and outputs availability

All supporting data (Tables S1–S10) are available in Borisova (2026, https://doi.org/10.5281/zenodo.18607217). Main text figures and table are available for download in the online version of this article.

Competing interests

The authors declare no competing interests.

Licence agreement

References

Aagaard P, Helgeson HC (1982). Thermodynamic and kinetic constraints on reaction rates among minerals and aqueous solutions: I. Theoretical considerations. *American Journal of Science* 282(3): 237–285. doi:10.2475/ajs.282.3.237.

Acosta-Vigil A, London D, Dewers TA, Morgan GB (2002). Dissolution of Corundum and Andalusite in H2O-Saturated Haplogranitic Melts at 800°C and 200 MPa: Constraints on Diffusivities and the Generation of Peraluminous Melts. *Journal of Petrology* 43(10): 1885–1908. doi:10.1093/petrology/43.10.1885.

Acosta-Vigil A, London D, Morgan GB (2006a). Experiments on the kinetics of partial melting of a leucogranite at 200 MPa H2O and 690-800°C: compositional variability of melts during the onset of H2O-saturated crustal anataxis. *Contributions to Mineralogy and Petrology* 151(5): 539–557. doi:10.1007/s00410-006-0081-8.

Acosta-Vigil A, London D, Morgan GB, Dewers TA (2006b). Dissolution of quartz, albite, and orthoclase in H2O-saturated haplogranitic melts at 800°C and 200 MPa: diffusive transport properties of granitic melts at crustal anatectic conditions. *Journal of Petrology* 47(2): 231–254. doi:10.1093/petrology/egi073.

Alexander CM (2011). Modeling diffusive dissolution in silicate melts. *Geochimica et Cosmochimica Acta* 75(2): 588–607. doi:10.1016/j.gca.2010.10.026.

Alkattan M, Oelkers EH, Dandurand JL, Schott J (1998). An experimental study of calcite and limestone dissolution rates as a function of pH from -1 to 3 and temperature from 25 to 80°C. *Chemical Geology* 151(1–4): 199–214. doi:10.1016/s0009-2541(98)00080-1.

Basch V, Godard M, Tommasi A, Rampone E (2025). Melt/rock ratios and melt fluxes during reactive percolation: from matrix- to melt-controlled dynamics. *Contributions to Mineralogy and Petrology* 180(6). doi:10.1007/s00410-024-02194-1.

Behrens H, Zhang Y (2001). Ar diffusion in hydrous silicic melts: implications for volatile diffusion mechanisms and fractionation. *Earth and Planetary Science Letters* 192(3): 363–376. doi:10.1016/s0012-821x(01)00458-7.

Berman RG (1988). Internally-Consistent Thermodynamic Data for Minerals in the System Na2O-K2O-CaO-MgO-FeO-Fe2O3-Al2O3-SiO2-TiO2-H2O-CO2. *Journal of Petrology* 29(2): 445–522. doi:10.1093/petrology/29.2.445.

Berner RA (1981). *Kinetics of weathering and diagenesis*, p. 111–134. De Gruyter. doi:10.1515/9781501508233-007.

Van den Bleeken G, Müntener O, Ulmer P (2010). Reaction processes between tholeiitic melt and residual peridotite in the uppermost mantle: an experimental study at 0.8 GPa. *Journal of Petrology* 51(1–2): 153–183. doi:10.1093/petrology/egp066.

Van den Bleeken G, Müntener O, Ulmer P (2011). Melt variability in percolated peridotite: an experimental study applied to reactive migration of tholeiitic basalt in the upper mantle. *Contributions to Mineralogy and Petrology* 161(6): 921–945. doi:10.1007/s00410-010-0572-5.

Bordère S, Glockner S (2021). Numerical modeling of diffusion-controlled phase transformation using the Darken method: Application to the dissolution/precipitation processes in materials. *Computational Materials Science* 186: 109944. doi:10.1016/j.commatsci.2020.109944.

Borghini G, Fumagalli P, Rampone E (2022). Melt–rock interactions in a veined mantle: pyroxenite–peridotite reaction experiments at 2 GPa. *European Journal of Mineralogy* 34(1): 109–129. doi:10.5194/ejm-34-109-2022.

Borisova A (2026). Experimental data on the dissolution of silicate minerals in geological and planetary melts. Version v4. Zenodo. doi:10.5281/zenodo.18607217.

Borisova AY (2022). Silica-rich melts originating from melt-hydrated peridotite reactions. *Lithos* 434–435: 106926. doi:10.1016/j.lithos.2022.106926.

Borisova AY, Bindeman IN, Toplis MJ, Zagrtdenov NR, Guignard J, Safonov OG, Bychkov AY, Shcheka S, Melnik OE, Marchelli M, Fehrenbach J (2020a). Zircon survival in shallow asthenosphere and deep lithosphere. *American Mineralogist* 105(11): 1662–1671. doi:10.2138/am-2020-7402.

Borisova AY, Bohrson WA (2023). How is carbonate crust digested by magma? *Frontiers in Earth Science* 11. doi:10.3389/feart.2023.1186207.

Borisova AY, Bohrson WA, Grégoire M (2017). Origin of primitive ocean island basalts by crustal gabbro assimilation and multiple recharge of plume-derived melts. *Geochemistry, Geophysics, Geosystems* 18(7): 2701–2716. doi:10.1002/2017gc006986.

Borisova AY, Bohrson WA, Spera FJ (2021a). Editorial: Magma-Rock and Magma-Mush Interactions as Fundamental Processes of Magmatic Differentiation. *Frontiers in Earth Science* 9. doi:10.3389/feart.2021.665588.

Borisova AY, Ceuleneer G, Kamenetsky VS, Arai S, Béjina F, Abily B, Bindeman IN, Polvé M, De Parseval P, Aigouy T, Pokrovski GS (2012). A New View on the Petrogenesis of the Oman Ophiolite Chromitites from Microanalyses of Chromite-hosted Inclusions. *Journal of Petrology* 53(12): 2411–2440. doi:10.1093/petrology/egs054.

Borisova AY, Lozovoy K, Pugliara A, Hungria T, Josse C, de Parseval P (2025). The Kinetic Control of Crystal Growth in Geological Reactions: An Example of Olivine–Ilmenite Assemblage. *Minerals* 15(6): 569. doi:10.3390/min15060569.

Borisova AY, Melnik OE, Gaborit N, Bindeman IN, Traillou T, Raffarin M, Stefánsson A, Laurent O, Leisen M, Llovet X, de Parseval P, Proietti A, Tait S (2023). In situ probing of the present-day zircon-bearing magma chamber at Krafla, Northeastern Iceland. *Frontiers in Earth Science* 11. doi:10.3389/feart.2023.1307303.

Borisova AY, Tilhac R (2021). Derivation of Hawaiian rejuvenated magmas from deep carbonated mantle sources: A review of experimental and natural constraints. *Earth-Science Reviews* 222: 103819. doi:10.1016/j.earscirev.2021.103819.

Borisova AY, Zagrtdenov NR, Toplis MJ, Bohrson WA, Nédélec A, Safonov OG, Pokrovski GS, Ceuleneer G, Bindeman IN, Melnik OE, Jochum KP, Stoll B, Weis U, Bychkov AY, Gurenko AA, Shcheka S, Terehin A, Polukeev VM, Varlamov DA, Chariteiro K, Gouy S, de Parseval P (2021b). Hydrated Peridotite – Basaltic Melt Interaction Part I: Planetary Felsic Crust Formation at Shallow Depth. *Frontiers in Earth Science* 9. doi:10.3389/feart.2021.640464.

Borisova AY, Zagrtdenov NR, Toplis MJ, Ceuleneer G, Safonov OG, Pokrovski GS, Jochum KP, Stoll B, Weis U, Shcheka S, Bychkov AY (2020b). Hydrated Peridotite–Basaltic Melt Interaction Part II: Fast Assimilation of Serpentinized Mantle by Basaltic Magma. *Frontiers in Earth Science* 8. doi:10.3389/feart.2020.00084.

Borisova AY, Zagrtdenov NR, Toplis MJ, Donovan JJ, Llovet X, Asimow PD, de Parseval P, Gouy S (2018). Secondary fluorescence effects in microbeam analysis and their impacts on geospeedometry and geothermometry. *Chemical Geology* 490: 22–29. doi:10.1016/j.chemgeo.2018.05.010.

Bowen N (1928). *The evolution of igneous rocks*. Princeton University Press, Princeton.

Brearley AJ (1987). An experimental and kinetic study of the breakdown of aluminous biotite at 800 °C: reaction microstructures and mineral chemistry. *Bulletin de Minéralogie* 110(5): 513–532. doi:10.3406/bulmi.1987.7994.

Brearley M, Scarfe CM (1986). Dissolution Rates of Upper Mantle Minerals in an Alkali Basalt Melt at High Pressure: An Experimental Study and Implications for Ultramafic Xenolith Survival. *Journal of Petrology* 27(5): 1157–1182. doi:10.1093/petrology/27.5.1157.

Bunsen R (1851). Ueber die Processe der vulkanischen Gesteinsbildungen Islands. *Annalen der Physik* 159(6): 197–272. doi:10.1002/andp.18511590602.

Burch T, Nagy K, Lasaga A (1993). Free energy dependence of albite dissolution kinetics at 80°C and pH 8.8. *Chemical Geology* 105(1–3): 137–162. doi:10.1016/0009-2541(93)90123-z.

Cambeses A, Chakraborty S, Jöns N, Montero P, Bea F (2023). How does inherited zircon survive in partially molten mantle: Insights on modes of magma transport in the mantle from nanoscale melt-crystal interaction experiments. *Earth and Planetary Science Letters* 601: 117911. doi:10.1016/j.epsl.2022.117911.

Casas AS, Hess KU, Badro J, Eitel M, Dingwell DB (2023). A redox effect on the viscosity of molten pyrolite. *Chemical Geology* 642: 121816. doi:10.1016/j.chemgeo.2023.121816.

Chakraborty S, Dingwell DB, Rubie DC (1995a). Multicomponent diffusion in ternary silicate melts in the system K_2O–Al_2O_3–SiO_2: I. Experimental measurements. *Geochimica et Cosmochimica Acta* 59(2): 255–264. doi:10.1016/0016-7037(94)00283-r.

Chakraborty S, Dingwell DB, Rubie DC (1995b). Multicomponent diffusion in ternary silicate melts in the system K_2O–Al_2O_3–SiO_2: II. Mechanisms, systematics, and geological applications. *Geochimica et Cosmochimica Acta* 59(2): 265–277. doi:10.1016/0016-7037(95)00284-7.

Chen Y, Zhang Y (2008). Olivine dissolution in basaltic melt. *Geochimica et Cosmochimica Acta* 72(19): 4756–4777. doi:10.1016/j.gca.2008.07.014.

Chen Y, Zhang Y (2009). Clinopyroxene dissolution in basaltic melt. *Geochimica et Cosmochimica Acta* 73(19): 5730–5747. doi:10.1016/j.gca.2009.06.016.

Claireaux C, Chopinet MH, Burov E, Gouillart E, Roskosz M, Toplis MJ (2016). Atomic mobility in calcium and sodium aluminosilicate melts at 1200 °C. *Geochimica et Cosmochimica Acta* 192: 235–247. doi:10.1016/j.gca.2016.07.032.

Cooper Jr A (1962). Dissolution kinetics in glass making. In *Advances in glass technology: Technical reports papers of the VI International Congress on Glass*, pp. 217–229. Plenum Press New York, Washington, D.C.

Cooper Jr A, Kingery W (1964). Dissolution in ceramic systems: I, molecular diffusion, natural convection, and forced convection studies of sapphire dissolution in calcium aluminium silicate. *Journal of the American Ceramic Society* 47(1): 37–43. doi:10.1111/j.1151-2916.1964.tb14638.x.

Cussler E (1997). *Diffusion: Mass Transfer in Fluid Systems*. Cambridge University Press, Cambridge, England.

Daly RA (1925). The Geology of Ascension Island. *Proceedings of the American Academy of Arts and Sciences* 60(1): 3. doi:10.2307/25130043.

Di Genova D, Bondar D, Zandonà A, Valdivia P, Al-Mukadam R, Fei H, Withers AC, Boffa Ballaran T, Kurnosov A, McCammon C, Deubener J, Katsura T (2023). Viscosity of anhydrous and hydrous peridotite melts. *Chemical Geology* 625: 121440. doi:10.1016/j.chemgeo.2023.121440.

Dingwell DB, Virgo D (1987). The effect of oxidation state on the viscosity of melts in the system Na2O-FeO-Fe2O3-SiO2. *Geochimica et Cosmochimica Acta* 51(2): 195–205. doi:10.1016/0016-7037(87)90231-6.

Dingwell DB, Webb SL (1990). Relaxation in silicate melts. *European Journal of Mineralogy* 2(4): 427–451. doi:10.1127/ejm/2/4/0427.

Donaldson CH (1985). The rates of dissolution of olivine, plagioclase, and quartz in a basalt melt. *Mineralogical Magazine* 49(354): 683–693. doi:10.1180/minmag.1985.049.354.07.

Donaldson CH (1990). Forsterite dissolution in superheated basaltic, andesitic and rhyolitic melts. *Mineralogical Magazine* 54(374): 67–74. doi:10.1180/minmag.1990.054.374.06.

Dunn T (1982). Oxygen diffusion in three silicate melts along the join diopside-anorthite. *Geochimica et Cosmochimica Acta* 46(11): 2293–2299. doi:10.1016/0016-7037(82)90202-2.

Edwards BR, Russell JK (1996). A review and analysis of silicate mineral dissolution experiments in natural silicate melts. *Chemical Geology* 130(3–4): 233–245. doi:10.1016/0009-2541(96)00025-3.

Edwards BR, Russell JK (1998). Time scales of magmatic processes: New insights from dynamic models for magmatic assimilation. *Geology* 26(12): 1103. doi:10.1130/0091-7613(1998)026<1103:tsompn>2.3.co;2.

Eyring H (1935). The Activated Complex in Chemical Reactions. *The Journal of Chemical Physics* 3(2): 107–115. doi:10.1063/1.1749604.

Ghiorso MS (1985). Chemical mass transfer in magmatic processes: I. Thermodynamic relations and numerical algorithms. *Contributions to Mineralogy and Petrology* 90(2–3): 107–120. doi:10.1007/bf00378254.

Ghiorso MS (1987). Chemical mass transfer in magmatic processes: III. Crystal growth, chemical diffusion and thermal diffusion in multicomponent silicate melts. *Contributions to Mineralogy and Petrology* 96(3): 291–313. doi:10.1007/bf00371250.

Ghiorso MS, Carmichael ISE, Rivers ML, Sack RO (1983). The Gibbs free energy of mixing of natural silicate liquids; an expanded regular solution approximation for the calculation of magmatic intensive variables. *Contributions to Mineralogy and Petrology* 84(2–3): 107–145. doi:10.1007/bf00371280.

Ghiorso MS, Gualda GAR (2015). An H2O–CO2 mixed fluid saturation model compatible with rhyolite-MELTS. *Contributions to Mineralogy and Petrology* 169(6). doi:10.1007/s00410-015-1141-8.

Ghiorso MS, Sack RO (1995). Chemical mass transfer in magmatic processes IV. A revised and internally consistent thermodynamic model for the interpolation and extrapolation of liquid-solid equilibria in magmatic systems at elevated temperatures and pressures. *Contributions to Mineralogy and Petrology* 119(2–3): 197–212. doi:10.1007/bf00307281.

Giordano D, Russell JK, Dingwell DB (2008). Viscosity of magmatic liquids: A model. *Earth and Planetary Science Letters* 271(1–4): 123–134. doi:10.1016/j.epsl.2008.03.038.

Gregory DP, Riddiford AC (1956). Transport to the surface of a rotating disc. *Journal of the Chemical Society (Resumed)* pp. 3756–3764. doi:10.1039/jr9560003756.

Gualda GAR, Ghiorso MS (2014). Phase-equilibrium geobarometers for silicic rocks based on rhyolite-MELTS. Part 1: Principles, procedures, and evaluation of the method. *Contributions to Mineralogy and Petrology* 168(1). doi:10.1007/s00410-014-1033-3.

Gualda GAR, Ghiorso MS, Lemons RV, Carley TL (2012). Rhyolite-MELTS: a Modified Calibration of MELTS Optimized for Silica-rich, Fluid-bearing Magmatic Systems. *Journal of Petrology* 53(5): 875–890. doi:10.1093/petrology/egr080.

Guo C, Zhang Y (2016). Multicomponent diffusion in silicate melts: SiO2-TiO2-Al2O3-MgO-CaO-Na2O-K2O system. *Geochimica et Cosmochimica Acta* 195: 126–141. doi:10.1016/j.gca.2016.09.003.

Guo C, Zhang Y (2020). Multicomponent diffusion in a basaltic melt: Temperature dependence. *Chemical Geology* 549: 119700. doi:10.1016/j.chemgeo.2020.119700.

Guy C, Schott J (1989). Multisite surface reaction versus transport control during the hydrolysis of a complex oxide. *Chemical Geology* 78(3–4): 181–204. doi:10.1016/0009-2541(89)90057-0.

Hammouda T, Pichavant M (1999). Kinetics of melting of fluorphlogopite-quartz pairs at 1 atmosphere. *European Journal of Mineralogy* 11(4): 637–654. doi:10.1127/ejm/11/4/0637.

Hammouda T, Pichavant M, Chaussidon M (1996). Isotopic equilibration during partial melting: an experimental test of the behaviour of Sr. *Earth and Planetary Science Letters* 144(1–2): 109–121. doi:10.1016/0012-821x(96)00144-6.

Harrison TM (1982). Diffusion of ^{40}Ar in hornblende. *Contributions to Mineralogy and Petrology* 78(3): 324–331. doi:10.1007/bf00398927.

Harrison TM, Watson EB (1983). Kinetics of zircon dissolution and zirconium diffusion in granitic melts of variable water content. *Contributions to Mineralogy and Petrology* 84(1): 66–72. doi:10.1007/bf01132331.

Jackson MD, Blundy J, Sparks RSJ (2018). Chemical differentiation, cold storage and remobilization of magma in the Earth's crust. *Nature* 564(7736): 405–409. doi:10.1038/s41586-018-0746-2.

Johannes W (1989). Melting of plagioclase-quartz assemblages at 2 kbar water pressure. *Contributions to Mineralogy and Petrology* 103(3): 270–276. doi:10.1007/bf00402914.

Kerr RC (1995). Convective crystal dissolution. *Contributions to Mineralogy and Petrology* 121(3): 237–246. doi:10.1007/bf02688239.

Kirkpatrick RJ (1981). *Kinetics of crystallization of igneous rocks*, p. 321–398. De Gruyter. doi:10.1515/9781501508233-012.

Klaver M, Klemme S, Liu XN, Hin RC, Coath CD, Anand M, Lissenberg CJ, Berndt J, Elliott T (2024). Titanium-rich basaltic melts on the Moon modulated by reactive flow processes. *Nature Geoscience* 17(2): 118–123. doi:10.1038/s41561-023-01362-5.

Kono Y, Kenney-Benson C, Hummer D, Ohfuji H, Park C, Shen G, Wang Y, Kavner A, Manning CE (2014). Ultralow viscosity of carbonate melts at high pressures. *Nature Communications* 5(1). doi:10.1038/ncomms6091.

Konrad-Schmolke M, Halama R, Wirth R, Thomen A, Klitscher N, Morales L, Schreiber A, Wilke FDH (2018). Mineral dissolution and reprecipitation mediated by an amorphous phase. *Nature Communications* 9(1). doi:10.1038/s41467-018-03944-z.

Kubicki JD, Lasaga AC (1991). Molecular dynamics and diffusion in silica melts. In *Diffusion, Atomic Ordering, and Mass Transport*, p. 1–50. Springer US. doi:10.1007/978-1-4613-9019-0_1.

Kuo LC, Kirkpatrick RJ (1985a). Dissolution of mafic minerals and its implications for the ascent velocities of peridotite-bearing basalt magmas. *The Journal of Geology* 93(6): 691–700. doi:10.1086/628996.

Kuo LC, Kirkpatrick RJ (1985b). Kinetics of crystal dissolution in the system diopside-forsterite-silica. *American Journal of Science* 285(1): 51–90. doi:10.2475/ajs.285.1.51.

Lasaga AC (1981). *Transition State Theory*, p. 135–170. De Gruyter. doi:10.1515/9781501508233-008.

Lasaga AC (1995). *Fundamental approaches in describing mineral dissolution and precipitation rates*, p. 23–86. De Gruyter. doi:10.1515/9781501509650-004.

Lasaga AC (1998). *Kinetic Theory in the Earth Sciences*. Princeton University Press. doi:10.1515/9781400864874.

Lasaga AC, Luttge A (2001). Variation of Crystal Dissolution Rate Based on a Dissolution Stepwave Model. *Science* 291(5512): 2400–2404. doi:10.1126/science.1058173.

Lesher C, Hervig R, Tinker D (1996). Self diffusion of network formers (silicon and oxygen) in naturally occurring basaltic liquid. *Geochimica et Cosmochimica Acta* 60(3): 405–413. doi:10.1016/0016-7037(95)00400-9.

Liang Y (1999). Diffusive dissolution in ternary systems: analysis with applications to quartz and quartzite dissolution in molten silicates. *Geochimica et Cosmochimica Acta* 63(23–24): 3983–3995. doi:10.1016/s0016-7037(99)00203-3.

Liang Y (2000). Dissolution in molten silicates: effects of solid solution. *Geochimica et Cosmochimica Acta* 64(9): 1617–1627. doi:10.1016/s0016-7037(00)00331-8.

Liang Y (2003). Kinetics of crystal-melt reaction in partially molten silicates: 1. Grain scale processes. *Geochemistry, Geophysics, Geosystems* 4. doi:10.1029/2002GC000375.

Liang Y, Richter FM, Chamberlin L (1997). Diffusion in silicate melts: III. Empirical models for multicomponent diffusion. *Geochimica et Cosmochimica Acta* 61(24): 5295–5312. doi:10.1016/s0016-7037(97)00301-3.

Liang Y, Richter FM, Watson EB (1996). Diffusion in silicate melts: II. Multicomponent diffusion in CaOAl2O3SiO2 at 1500°C and 1 GPa. *Geochimica et Cosmochimica Acta* 60(24): 5021–5035. doi:10.1016/s0016-7037(96)00352-3.

Lin Y, van Westrenen W, Mao HK (2021). Oxygen controls on magmatism in rocky exoplanets. *Proceedings of the National Academy of Sciences* 118(45). doi:10.1073/pnas.2110427118.

Lin Y, van Westrenen W, Mao HK (2022). Reply to Walker et al.: Rock melting? Oxygen matters. *Proceedings of the National Academy of Sciences* 119(41). doi:10.1073/pnas.2211778119.

London D, Morgan GB, Acosta-Vigil A (2012). Experimental simulations of anatexis and assimilation involving metapelite and granitic melt. *Lithos* 153: 292–307. doi:10.1016/j.lithos.2012.04.006.

Lundstrom CC (2000). Rapid diffusive infiltration of sodium into partially molten peridotite. *Nature* 403(6769): 527–530. doi:10.1038/35000546.

Morgan Z, Liang Y (2003). An experimental and numerical study of the kinetics of harzburgite reactive dissolution with applications to dunite dike formation. *Earth and Planetary Science Letters* 214(1–2): 59–74. doi:10.1016/s0012-821x(03)00375-3.

Morgan Z, Liang Y (2005). An experimental study of the kinetics of lherzolite reactive dissolution with applications to melt channel formation. *Contributions to Mineralogy and Petrology* 150(4): 369–385. doi:10.1007/s00410-005-0033-8.

Morgan Z, Liang Y, Hess P (2006). An experimental study of anorthosite dissolution in lunar picritic magmas: Implications for crustal assimilation processes. *Geochimica et Cosmochimica Acta* 70(13): 3477–3491. doi:10.1016/j.gca.2006.04.027.

Mungall JE (2002). Empirical models relating viscosity and tracer diffusion in magmatic silicate melts. *Geochimica et Cosmochimica Acta* 66(1): 125–143. doi:10.1016/s0016-7037(01)00736-0.

Mysen B, Virgo D, Scarfe C (1979). Viscosity of silicate melts as a function of pressure: structural interpretation. *Carnegie Institution of Washington Yearbook* 78: 551–556.

Nagy K, Lasaga A (1992). Dissolution and precipitation kinetics of gibbsite at 80°C and pH 3: The dependence on solution saturation state. *Geochimica et Cosmochimica Acta* 56(8): 3093–3111. doi:10.1016/0016-7037(92)90291-p.

Nowak M, Schreen D, Spickenbom K (2004). Argon and CO2 on the race track in silicate melts: A tool for the development of a CO2 speciation and diffusion model. *Geochimica et Cosmochimica Acta* 68(24): 5127–5138. doi:10.1016/j.gca.2004.06.002.

Oishi Y, Cooper Jr A, Kingery W (1965). Dissolution in ceramic systems: iii, Boundary layer concentration gradient. *Journal of the American Ceramic Society* 48(2): 88–95. doi:10.1111/j.1151-2916.1965.tb11805.x.

Pablo H, Schuller S, Toplis M, Mostefaoui S, Mesbah A, Roskosz M (2019). Impact of chemical diffusion on crystal growth in sodium borosilicate glasses. *Journal of Non-Crystalline Solids* 503–504: 313–322. doi:10.1016/j.jnoncrysol.2018.10.013.

Pec M, Holtzman BK, Zimmerman M, Kohlstedt DL (2015). Reaction infiltration instabilities in experiments on partially molten mantle rocks. *Geology* 43(7): 575–578. doi:10.1130/g36611.1.

Pec M, Holtzman BK, Zimmerman ME, Kohlstedt DL (2017). Reaction Infiltration Instabilities in Mantle Rocks: an Experimental Investigation. *Journal of Petrology* 58(5): 979–1003. doi:10.1093/petrology/egx043.

Pec M, Holtzman BK, Zimmerman ME, Kohlstedt DL (2020). Influence of Lithology on Reactive Melt Flow Channelization. *Geochemistry, Geophysics, Geosystems* 21(8). doi:10.1029/2020gc008937.

Pichavant M, Hammouda T, Scaillet B (1996). Control of redox state and Sr isotopic composition of granitic magmas: a critical evaluation of the role of source rocks. *Earth and Environmental Science Transactions of the Royal Society of Edinburgh* 87(1–2): 321–329. doi:10.1017/s0263593300006714.

Roskosz M, Toplis MJ, Besson P, Richet P (2005). Nucleation mechanisms: A crystal-chemical investigation of phases forming in highly supercooled aluminosilicate liquids. *Journal of Non-Crystalline Solids* 351(14–15): 1266–1282. doi:10.1016/j.jnoncrysol.2005.02.021.

Roskosz M, Toplis MJ, Richet P (2006). Crystallization of Highly Supercooled Silicate Melts. *Advanced Engineering Materials* 8(12): 1224–1228. doi:10.1002/adem.200600181.

Rospabé M, Ceuleneer G, Granier N, Arai S, Borisova AY (2019). Multi-scale development of a stratiform chromite ore body at the base of the dunitic mantle-crust transition zone (Maqsad diapir, Oman ophiolite): The role of repeated melt and fluid influxes. *Lithos* 350–351: 105235. doi:10.1016/j.lithos.2019.105235.

Rubie DC, Brearley AJ (1987). Metastable melting during the breakdown of muscovite + quartz at 1 kbar. *Bulletin de Minéralogie* 110(5): 533–549. doi:10.3406/bulmi.1987.7995.

Scarfe C, Takahashi E, Yoder H (1980). Rates of dissolution of upper mantle minerals in an alkali-olivine basalt melt at high pressures. *Carnegie Institution* 79: 290–296.

Scherer G, Vergano PJ, Uhlmann DR (1970). A study of quartz melting. *Physics and Chemistry of Glasses* 11: 53–58.

Schott J, Oelkers EH, Bénézeth P, Goddéris Y, François L (2012). Can accurate kinetic laws be created to describe chemical weathering? *Comptes Rendus Géoscience* 344(11–12): 568–585. doi:10.1016/j.crte.2012.10.005.

Schott J, Pokrovsky OS, Oelkers EH (2009). The Link Between Mineral Dissolution/Precipitation Kinetics and Solution Chemistry. *Reviews in Mineralogy and Geochemistry* 70(1): 207–258. doi:10.2138/rmg.2009.70.6.

Shaw CSJ (1999). Dissolution of orthopyroxene in basanitic magma between 0.4 and 2 GPa: further implications for the origin of Si-rich alkaline glass inclusions in mantle xenoliths. *Contributions to Mineralogy and Petrology* 135(2–3): 114–132. doi:10.1007/s004100050501.

Shaw CSJ (2000). The effect of experiment geometry on the mechanism and rate of dissolution of quartz in basanite at 0.5 GPa and 1350 °C. *Contributions to Mineralogy and Petrology* 139(5): 509–525. doi:10.1007/s004100000153.

Shaw CSJ (2004). Mechanisms and rates of quartz dissolution in melts in the CMAS (CaO-MgO-Al2O3-SiO2) system. *Contributions to Mineralogy and Petrology* 148(2): 180–200. doi:10.1007/s00410-004-0581-3.

Shaw CSJ (2006). Effects of melt viscosity and silica activity on the rate and mechanism of quartz dissolution in melts of the CMAS and CAS systems. *Contributions to Mineralogy and Petrology* 151(6): 665–680. doi:10.1007/s00410-006-0086-3.

Shaw CSJ (2012). The effects of potassium addition on the rate of quartz dissolution in the CMAS and CAS systems. *Contributions to Mineralogy and Petrology* 164(5): 839–857. doi:10.1007/s00410-012-0777-x.

Shaw CSJ, Dingwell DB (2008). Experimental peridotite–melt reaction at one atmosphere: a textural and chemical study. *Contributions to Mineralogy and Petrology* 155(2): 199–214. doi:10.1007/s00410-007-0237-1.

Shaw CSJ, Klausen KB, Mao H (2018). Kinetics of dissolution of sapphire in melts in the CaO–Al2O3–SiO2 system. *Geochimica et Cosmochimica Acta* 229: 129–146. doi:10.1016/j.gca.2018.03.011.

Shaw CSJ, Thibault Y, Edgar AD, Lloyd FE (1998). Mechanisms of orthopyroxene dissolution in silica-undersaturated melts at 1 atmosphere and implications for the origin of silica-rich glass in mantle xenoliths. *Contributions to Mineralogy and Petrology* 132(4): 354–370. doi:10.1007/s004100050429.

Shaw HR (1972). Viscosities of magmatic silicate liquids; an empirical method of prediction. *American Journal of Science* 272(9): 870–893. doi:10.2475/ajs.272.9.870.

Shiraki R, Brantley SL (1995). Kinetics of near-equilibrium calcite precipitation at 100°C: An evaluation of elementary reaction-based and affinity-based rate laws. *Geochimica et Cosmochimica Acta* 59(8): 1457–1471. doi:10.1016/0016-7037(95)00055-5.

Thomson AR, Walter MJ, Kohn SC, Brooker RA (2016). Slab melting as a barrier to deep carbon subduction. *Nature* 529(7584): 76–79. doi:10.1038/nature16174.

Thornber C, Huebner J (1982). Dissolution rates of olivine in basaltic liquids. *EOS* 63: 452–453.

Thornber C, Huebner J (1985). Dissolution of olivine in basaltic liquids: experimental observations and applications. *American Mineralogist* 70: 934–945.

Trial AF, Spera FJ (1994). Measuring the multicomponent diffusion matrix: Experimental design and data analysis for silicate melts. *Geochimica et Cosmochimica Acta* 58(18): 3769–3783. doi:10.1016/0016-7037(94)90362-x.

Tsuchiyama A (1985a). Dissolution kinetics of plagioclase in the melt of the system diopside-albite-anorthite, and origin of dusty plagioclase in andesites. *Contributions to Mineralogy and Petrology* 89(1): 1–16. doi:10.1007/bf01177585.

Tsuchiyama A (1985b). Partial melting kinetics of plagioclase-diopside pairs. *Contributions to Mineralogy and Petrology* 91(1): 12–23. doi:10.1007/bf00429423.

Tsuchiyama A (1986). Melting and dissolution kinetics: Application to partial melting and dissolution of xenoliths. *Journal of Geophysical Research: Solid Earth* 91(B9): 9395–9406. doi:10.1029/jb091ib09p09395.

Tsuchiyama A, Takahashi E (1983). Melting kinetics of a plagioclase feldspar. *Contributions to Mineralogy and Petrology* 84(4): 345–354. doi:10.1007/bf01160286.

Tursack E, Liang Y (2012). A comparative study of melt-rock reactions in the mantle: laboratory dissolution experiments and geological field observations. *Contributions to Mineralogy and Petrology* 163(5): 861–876. doi:10.1007/s00410-011-0703-7.

Van Orman JA, Grove TL (2000). Origin of lunar high-titanium ultramafic glasses: Constraints from phase relations and dissolution kinetics of clinopyroxene-ilmenite cumulates. *Meteoritics & Planetary Science* 35(4): 783–794. doi:10.1111/j.1945-5100.2000.tb01462.x.

Wagstaff FE (1969). Crystallization and Melting Kinetics of Cristobalite. *Journal of the American Ceramic Society* 52(12): 650–654. doi:10.1111/j.1151-2916.1969.tb16069.x.

Wang C, Liang Y, Xu W, Dygert N (2013). Effect of melt composition on basalt and peridotite interaction: laboratory dissolution experiments with applications to mineral compositional variations in mantle xenoliths from the North China Craton. *Contributions to Mineralogy and Petrology* 166(5): 1469–1488. doi:10.1007/s00410-013-0938-6.

Wang C, Lo Cascio M, Liang Y, Xu W (2020). An experimental study of peridotite dissolution in eclogite-derived melts: Implications for styles of melt-rock interaction in lithospheric mantle beneath the North China Craton. *Geochimica et Cosmochimica Acta* 278: 157–176. doi:10.1016/j.gca.2019.09.022.

Watson EB (1982). Basalt contamination by continental crust: Some experiments and models. *Contributions to Mineralogy and Petrology* 80(1): 73–87. doi:10.1007/bf00376736.

Watson EB, Harrison TM (1984). Accessory minerals and the geochemical evolution of crustal magmatic systems: a summary and prospectus of experimental approaches. *Physics of the Earth and Planetary Interiors* 35(1–3): 19–30. doi:10.1016/0031-9201(84)90031-1.

Watson EB, Jurewicz SR (1984). Behavior of Alkalies during Diffusive Interaction of Granitic Xenoliths with Basaltic Magma. *The Journal of Geology* 92(2): 121–131. doi:10.1086/628843.

Wise DL, Houghton G (1966). The diffusion coefficients of ten slightly soluble gases in water at 10-60°C. *Chemical Engineering Science* 21(11): 999–1010. doi:10.1016/0009-2509(66)85096-0.

Wolf GH, McMillan PF (1995). Pressure effects on silicate melt structure and properties. In *Structure, Dynamics, and Properties of Silicate Melts*, vol. 32 of *Reviews in Mineralogy*, p. 505–562. De Gruyter. doi:10.1515/9781501509384-013.

Yoshizawa FT, Garel-Laurin AC, Burov E, Toplis MJ (2025). Diffusive dissolution of α-alumina in industrial soda-lime silica glass. *Journal of Non-Crystalline Solids* 650: 123351. doi:10.1016/j.jnoncrysol.2024.123351.

Yu Y, Zhang Y, Chen Y, Xu Z (2016). Kinetics of anorthite dissolution in basaltic melt. *Geochimica et Cosmochimica Acta* 179: 257–274. doi:10.1016/j.gca.2016.02.002.

Yu Y, Zhang Y, Yang Y (2019). Kinetics of Quartz Dissolution in Natural Silicate Melts and Dependence of SiO2 Diffusivity on Melt Composition. *ACS Earth and Space Chemistry* 3(4): 599–616. doi:10.1021/acsearthspacechem.8b00193.

Zagrtdenov N, Borisova A, Toplis M, Duployer B, Tenailleau C (2015). Preliminary experimental investigation of chromite dissolution in mid-ocean ridge basalt melt. In *Proceedings of the Goldschmidt Conference, Prague, Czech Republic*, p. 16–21.

Zagrtdenov NR, Ceuleneer G, Rospabé M, Borisova AY, Toplis MJ, Benoit M, Abily B (2018). Anatomy of a chromitite dyke in the mantle/crust transition zone of the Oman ophiolite. *Lithos* 312–313: 343–357. doi:10.1016/j.lithos.2018.05.012.

Zhang Y (2008). *Geochemical kinetics*. Princeton University Press, Princeton, New Jersey, USA.

Zhang Y (2010). Diffusion in Minerals and Melts: Theoretical Background. *Reviews in Mineralogy and Geochemistry* 72(1): 5–59. doi:10.2138/rmg.2010.72.2.

Zhang Y (2013). Kinetics and dynamics of mass-transfer-controlled mineral and bubble dissolution or growth: a review. *European Journal of Mineralogy* 25(3): 255–266. doi:10.1127/0935-1221/2013/0025-2292.

Zhang Y, Gan T (2022). Diffusion in Melts and Magmas. *Reviews in Mineralogy and Geochemistry* 87(1): 283–337. doi:10.2138/rmg.2022.87.07.

Zhang Y, Walker D, Lesher CE (1989). Diffusive crystal dissolution. *Contributions to Mineralogy and Petrology* 102(4): 492–513. doi:10.1007/bf00371090.

Zhang Y, Xu Z (2003). Kinetics of convective crystal dissolution and melting, with applications to methane hydrate dissolution and dissociation in seawater. *Earth and Planetary Science Letters* 213(1–2): 133–148. doi:10.1016/s0012-821x(03)00297-8.

Zhang Y, Xu Z (2016). Zircon saturation and Zr diffusion in rhyolitic melts, and zircon growth geospeedometer. *American Mineralogist* 101(6): 1252–1267. doi:10.2138/am-2016-5462.